Cellular/Molecular

Opioid-Induced Hyperalgesia and Tolerance Are Driven by HCN Ion Channels

Xue Han, Larissa Garcia Pinto, Bruno Vilar, and Peter A. McNaughton
Wolfson Sensory, Pain and Regeneration Centre, King's College London, London SE1 1UL, United Kingdom

Prolonged exposure to opioids causes an enhanced sensitivity to painful stimuli (opioid-induced hyperalgesia, OIH) and a need for increased opioid doses to maintain analgesia (opioid-induced tolerance, OIT), but the mechanisms underlying both processes remain obscure. We found that pharmacological block or genetic deletion of HCN2 ion channels in primary nociceptive neurons of male mice completely abolished OIH but had no effect on OIT. Conversely, pharmacological inhibition of central HCN channels alleviated OIT but had no effect on OIH. Expression of C-FOS, a marker of neuronal activity, was increased in second-order neurons of the dorsal spinal cord by induction of OIH, and the increase was prevented by peripheral block or genetic deletion of HCN2, but block of OIT by spinal block of HCN channels had no impact on C-FOS expression in dorsal horn neurons. Collectively, these observations show that OIH is driven by HCN2 ion channels in peripheral nociceptors, while OIT is driven by a member of the HCN family located in the CNS. Induction of OIH increased cAMP in nociceptive neurons, and a consequent shift in the activation curve of HCN2 caused an increase in nociceptor firing. The shift in HCN2 was caused by expression of a constitutively active μ-opioid receptor (MOR) and was reversed by MOR antagonists. We identified the opioid-induced MOR as a six-transmembrane splice variant, and we show that it increases cAMP by coupling constitutively to G_s. HCN2 ion channels therefore drive OIH, and likely OIT, and may be a novel therapeutic target for the treatment of addiction.

Key words: addiction; HCN ion channels; hyperalgesia; μ-opioid receptor; opioid; opioid tolerance

Significance Statement

Chronic opioid treatment causes opioid-induced hyperalgesia (OIH) and opioid-induced tolerance (OIT), both important drivers of opioid addiction. Here we show that an ion channel named HCN2 causes OIH, because blocking or genetically deleting HCN2 suppresses OIH. The activity of HCN2 is enhanced by chronic opioid exposure, resulting in increased excitability of peripheral nociceptive (pain-sensing) neurons. The enhanced HCN2 activity is caused by expression of an aberrant alternatively spliced μ-opioid receptor that increases intracellular cAMP, that in turn binds to and directly activates HCN2 ion channels. Conversely, we find that a member of the HCN ion channel family expressed in the CNS drives OIT, probably by a similar mechanism. HCN channels are therefore potential therapeutic targets for the treatment of both OIH and OIT.

Introduction

Chronic opioid exposure can cause opioid-induced hyperalgesia (OIH), a hypersensitivity to painful stimuli following long-term opioid exposure (Santonocito et al., 2018), and also opioid-induced tolerance (OIT), in which opioid analgesic potency fades with repeated administration. Many studies have proposed that OIH originates within the CNS, based on the idea that "central sensitization" is an important driver of pain (reviewed in Latremoliere and Woolf, 2009). Proposals for the mechanism of central sensitization induced by chronic opioid exposure include long-term potentiation of NMDA ion channels in the spinal dorsal horn (Zeng et al., 2006; Drdla et al., 2009; Zhao et al., 2012; Li et al., 2013; Wang et al., 2015; Deng et al., 2019; Li et al., 2019) or in the periaqueductal gray (Ghelardini

Received July 21, 2023; revised Oct. 24, 2023; accepted Nov. 19, 2023.

Author contributions: X.H. and P.A.M. designed research; X.H., L.G.P., and B.V. performed research; X.H., L.G.P., and P.A.M. analyzed data; X.H. wrote the first draft of the paper; P.A.M. edited the paper.

We thank Carl Hobbs for assisting with immunohistochemistry, Alice Fuller for carrying out the blinding process in behavioral assays, and Chris Tsantoulas for comments on the MS. This work was supported by grants from the Wellcome Trust to P.A.M (Investigator Award 205006/Z/16/Z) and a China Scholarship Council (CSC) PhD studentship award to X.H. X.H. and P.A.M. planned the study and wrote the manuscript. X.H. performed behavioral experiments, patch-clamping, immunohistochemistry, ELISA, and qPCR. L.G.P. performed qPCR and ELISA.

P.A.M. is co-author of the following patents describing HCN2-selective ion channel blockers: WO 2022/185055; WO 2022/185057; WO 2022/185058.

Correspondence should be addressed to Xue Han at hanxue19890123@hotmail.com or Peter McNaughton at peter.mcnaughton@kcl.ac.uk.

X.H.'s present address: Department of Pain Medicine, The Second Affiliated Hospital of Guangzhou Medical University, Guangzhou 510260, China.

https://doi.org/10.1523/JNEUROSCI.1368-23.2023

et al., 2008; Mo et al., 2023). An alternative proposal is that microglial activation may drive OIH (Ferrini et al., 2013; Trang et al., 2015; Reiss et al., 2022). Corder et al. (2017), however, found no evidence for expression of opioid receptors in spinal microglia, and Arout et al. (2019) found no effect in clinical trials of minocycline, an inhibitor of microglial activation, on OIH.

Recent studies have shown instead that long-term exposure to μ-opioid receptor (MOR) agonists causes peripheral nociceptor sensitization, manifested as a reduced threshold and increased frequency of spontaneous discharge in primary nociceptive neurons, and that inhibiting nociceptor sensitization inhibits OIH (Hogan et al., 2013; Gong et al., 2016; Khomula et al., 2019). Critically, genetic deletion of MORs in peripheral nociceptors, or block of peripheral μ-opioid receptors by the use of a peripherally restricted μ-opioid antagonist, completely abolished both OIH and spinal LTP (Corder et al., 2017; Sun et al., 2019). These results support the idea that peripheral MORs are the primary drivers of OIH and that the effects on OIH of the CNS interventions outlined above are due to central modulation of a pain signal initiated in peripheral nociceptors.

In the present paper, we explore the possibility that hyperpolarization-activated, cyclic nucleotide-gated (HCN) channels may drive both OIH and OIT. HCN channels are activated by membrane hyperpolarization in the range between −60 and −100 mV, and activation is potentiated by direct binding of cyclic nucleotides (reviewed in Tsantoulas et al., 2016). The inward current generated by HCN ion channels is usually referred as I_h in neurons, where it controls neuronal resting potentials and firing frequency (Chan et al., 2004).

The HCN ion channel family consists of four different genes, HCN1 to HCN4 (Gauss et al., 1998; Ludwig et al., 1998; Kaupp and Seifert, 2001). Activation of HCN2 and HCN4 is potentiated by elevated cyclic adenosine monophosphate (cAMP), that binds directly to a C-terminal cyclic nucleotide binding domain (CNBD). HCN1 and HCN3, on the other hand, are relatively insensitive to cAMP (Sartiani et al., 2017). Large non-nociceptive somatosensory neurons express mainly HCN1 (Momin et al., 2008), while small nociceptive C-fiber neurons express HCN2 and HCN3 (Tu et al., 2004; Kouranova et al., 2008; Emery et al., 2011; Lainez et al., 2019). HCN2 channels play a critical role in modulating the excitability of nociceptive primary sensory neurons and are responsible for the development of several types of chronic pain (Emery et al., 2011, 2012; Schnorr et al., 2014; Young et al., 2014; Tsantoulas et al., 2016, 2017, 2022). It is unknown, though, whether HCN2 channels are involved in OIH and OIT.

Inhibition of the I_h current may be a mechanism by which opioids relieve pain in the short term (Ingram and Williams, 1994), while long-term opioid exposure enhances cAMP levels and thus might cause OIH (Bie et al., 2005). The above findings provide a clue that HCN channels may participate not only in the acute antinociceptive effect of opioids but also in side effects following chronic opioid exposure, such as OIT and OIH. In the present study, we explored the possible involvement of HCN channels in both OIH and OIT.

Materials and Methods

Animals

Adult C57BL/6 mice (6–9 weeks old, Charles River), the conditional *hcn2* knock-out ($na_v1.8\text{-}cre^{+/-}$/f$hcn2^{+/+}$, *hcn2* cKO), in which *hcn2* deletion was targeted to nociceptive ($Na_V1.8$-expressing) dorsal root ganglion (DRG) neurons, and floxed littermate mice ($Na_V1.8\text{-}Cre^{-/-}$/fHCN2$^{+/+}$, fHCN2; 6–10 weeks old) were used in this study. The transgenic mice had been backcrossed onto the WT C57BL/6 strain for six generations (for detailed description, see Emery et al., 2011). The genotypes of transgenic mice were confirmed by quantitative PCR (qPCR; Transnetyx) and were double-checked by immunohistochemistry (Fig 2-1). The specificity of the HCN2 antibody was validated by the complete absence of HCN2 staining in DRG from HCN2 global knock-out mice (Fig 5-1). All mice were housed 4–5 per cage in a temperature-controlled environment where a 12 h light/dark cycle is maintained and were provided with food and water *ad libitum*. Before starting each experiment, all animals acclimatized to the cage environment for at least 1 week. All procedures were approved by the Animal Welfare Ethical Review Board (AWERB) of KCL and carried out in accordance with the Home Office (UK) regulations and the Animals (Scientific Procedures) Act 1986, as well as being compliant with the recommendations of the Committee for Research and Ethical Issues of the International Association for the Study of Pain (IASP).

Opioid-induced hyperalgesia and tolerance models

In vivo OIH and OIT models were developed in which morphine (10 mg/kg) was administered once per day for 10 d to WT mice and transgenic (fHCN2 and HCN2 cKO) mice subcutaneously, with an injection volume of 10 μl/g body weight. Drug dilutions and vehicle used Dulbecco's phosphate-buffered saline (DPBS).

Behavioral assays

In order to ensure objectivity, the primary experimenter was blinded to treatments. All drugs were given to the experimenter in coded tubes, and their identity was decoded only after the completion of behavioral tests. Mice were acclimatized for 60–90 min to the behavioral apparatus in an isolated, temperature- and light-constant room. Behavioral testing was conducted between 10:00 A.M. and 5:00 P.M.

Drug treatment. Ivabradine (Sigma SML0281) was diluted in DPBS and delivered subcutaneously (5 mg/kg, injection volume 10 μl/g body weight) as a single injection. H-89 dihydrochloride (H89, Tocris 2910) and methylnaltrexone bromide (MNB, Sigma SML0277) were dissolved into stock solutions at 10 mg/ml, and further dilutions were made in DPBS. H89 (5 mg/kg), MNB (5 mg/kg), or vehicle (DPBS) were injected subcutaneously at a volume of 10 μl/g body weight as described in Results.

Assaying mechanical hyperalgesia. Paw withdrawal mechanical threshold was quantified using a dynamic plantar aesthesiometer (Ugo Basile 37450). Once exploratory behavior had ceased, the filament was positioned under the plantar hindpaw surface and the actuator (0.5 mm diameter) automatically delivered an increasing mechanical stimulation (0–5 g) until a positive reaction was elicited, which was characterized as a sudden paw withdrawal, licking, and/or paw flinching. Paw withdrawal mechanical thresholds were averaged over at least three measurements with an interval of 5 min and a change of right/left paws. The filament actuator was calibrated with 5 and 50 g calibration weights prior to commencing the experiment each day. Having obtained baseline nociceptive measurements, paw withdrawal thresholds were measured every other day, immediately *before* the daily morphine injection, to monitor the development of opioid-induced mechanical hyperalgesia as free as possible from the effects of the previous morphine injection. After mechanical OIH had developed, the following tests were carried out, as required by the individual experiment: (1) for the assessment of the effect of peripheral injections of ivabradine (5 mg/kg, s.c.), we measured the mechanical thresholds before and 30, 60, and 120 min after injection; (2) to test whether central HCN channels are involved in mechanical OIH, we measured the mechanical thresholds before and 30 min after the intrathecal delivery of ivabradine (5 μl, 60 μM); and (3) to observe whether the protein kinase A (PKA) signaling pathway is implicated in OIH, we measured the mechanical thresholds 30 min after subcutaneous injection of H89, a PKA inhibitor. In addition, the role of peripheral MORs in mechanical OIH was assessed by subcutaneous injection of morphine combined with MNB (5 mg/kg), a peripherally restricted MOR antagonist, for 10 d.

Assaying thermal hyperalgesia: Hargreaves test. Thermal withdrawal latency was assessed with the Hargreaves test (IITC Plantar Analgesia Meter, IITC Life Science). Animals were allowed to move freely for 60–90 min in a quiet environment on a glass panel with a heating temperature preset to 30°C. When exploration had ceased, the trial was initiated by delivering a heat source (infrared light) to a hindpaw. The latency (s) to the first occurrence of a positive response (lick or flinching) was recorded. Paw withdrawal latencies were averaged over at least three measurements with an interval of 5 min and a change of right/left paws. The activating light intensity was set to 20%, idle light intensity was 2%, and a 20 s cutoff time was applied to prevent tissue damage. To determine the development of opioid-induced thermal hyperalgesia, we measured the thermal withdrawal thresholds every other day immediately *before* the next morphine injection. After thermal OIH had developed, in order to test the effect of ivabradine on thermal hyperalgesia, the Hargreaves test was performed before and 30, 60, and 120 min after the injection of ivabradine. The role of peripheral MORs in thermal OIH was assessed by subcutaneous injection of morphine combined with the peripherally restricted MOR antagonist MNB (5 mg/kg), for 10 d.

Assaying thermal opioid analgesia: hotplate test. The development of OIT was assessed with the hotplate test (The Hot/Cold Plate Analgesia Meter, Harvard Apparatus). Briefly, the plate temperature was set to 52°C and a 45 s cutoff was applied to prevent tissue damage. Mice were placed on the plate, and latency (s) to the first occurrence of a positive response (lick or flinching of hind paws) was recorded. To determine the development of opioid-induced thermal nociceptive tolerance, we measured the thermal withdrawal latency 30 min *after* morphine injection. After OIT had developed, (1) we injected morphine subcutaneously followed by ivabradine (two separate injections given one after the other) and the heat withdrawal latency was recorded 30 min after injection to observe whether s.c. ivabradine reverses OIT; (2) to assess whether central HCN channels are implicated in OIT, following the induction of OIT, we treated mice with an intrathecal ivabradine injection followed immediately by a subcutaneous morphine injection, and thermal withdrawal thresholds were measured 30 min after injection. To ensure appropriate delivery of the intrathecal injection, we included methylene blue (Sigma 77515, 1:1) with every injection, and the presence of methylene blue in the intrathecal space, and its absence in any other tissues adjacent to the spinal column, was verified post mortem.

The role of peripheral MORs in OIT was assessed by subcutaneous injection of morphine combined with the peripherally restricted opioid antagonist MNB (5 mg/kg) for 10 d as above, and thermal thresholds were measured 30 min after each injection to observe whether blocking peripheral MORs inhibited the development of OIT.

Immunohistochemistry

Mice were anesthetized with pentobarbital (Euthatal, Merial) and transcardially perfused with 4% paraformaldehyde (P6148, Sigma-Aldrich) in 0.1 M phosphate buffer, pH 7.4. Tissue was dissected and post-fixed at 4°C (DRG, 30 min; spinal cord, 2 h) followed by impregnation with 30% sucrose at 4°C for 24–48 h (or until tissue had sunk to the bottom of the well). Tissue was embedded in O.C.T. embedding medium (Thermo Scientific), rapidly frozen in liquid nitrogen, and stored in a −80°C freezer. Sections were cut in a cryostat at the required thickness (DRG, 10 µm; spinal cord, 20 µm), and 5–10 sections were adhered onto slides (SuperFrost Plus Adhesion Microscope Slides, Fisher Scientific).

Before antibody staining, sections were washed with PBST (PBS + 0.3% Triton X-100) three times at room temperature for 5 min. Nonspecific immunoreactivity was blocked by 5 min incubation in blocking buffer (PBST + 5% BSA + 5% donkey serum + 4% goat serum), and then slides were incubated overnight at 4°C with the primary antibody solution (diluted as below in blocking buffer). Primary antibodies used were mouse anti-HCN2 (1:500, Neuromab 75-111), rabbit anti-HCN2 (1:1,000, Alomone APC-030), rabbit anti-µ-opioid receptor (1:250, Abcam #ab134054), mouse anti-$Na_V1.8$ (1:1,000, Neuromab N134/12), rabbit anti-c-fos (1:1,000, Cell Signaling #2250), chicken anti-β3tubulin (1:1,000, Abcam #ab41489), and mouse anti-NeuN (1:1,000, Abcam #ab104224). The next day, slides were washed with PBST three times at room temperature (each wash for 10 min) and incubated for 1 h with the appropriate secondary antibodies: donkey anti-rabbit IgG (H + L) cross-adsorbed to Alexa Fluor 594, goat anti-chicken IgG (H + L) cross-adsorbed to Alexa Fluor 488, goat anti-mouse IgG-conjugated Alexa Fluor 488, or goat anti-mouse IgG2a cross-adsorbed to Alexa Fluor 488 (all 1:1,000, Invitrogen). Finally, slides were mounted with FluorSave mounting reagent (345789, Merck Life Science UK).

Image analysis. Antibody staining was imaged using a Zeiss Axioplan2 microscope with a digital camera and Axiovision software (Zeiss). Analysis of immunofluorescence was performed with FIJI (ImageJ) software. For quantification of HCN2 staining, three background intensity measurements were taken and mean intensity of background (BG) and its standard deviation (SD) were calculated in each image; a positive cell was then defined when its immunoreactivity intensity was stronger than 2BG + 2SD. These objective criteria compare well with subjective criteria of positively stained cells. Images were acquired from at least five sections (>250 cell profiles) per animal by using a 20× objective. Only cells having a visible nucleus were counted, to ensure that cell diameter was correctly quantified. Measurements of c-*fos* activation in the spinal cord were carried out by counting the number of C-FOS-positive neurons in the lumbar dorsal horn using a 20× objective in at least five spinal cord sections per animal.

cAMP ELISA

cAMP was quantified using a commercial ELISA kit (Cayman Chemical 501040). Briefly, DRG (L3–L5 both sides) were rapidly collected and flash-frozen on dry ice (within 5 min of mouse death). Frozen DRGs were dropped into 300 µl cold hydrochloric acid solution (Sigma, 2104) and homogenized on ice. Samples were centrifuged at $1,500 \times g$ for 10 min, and supernatants were transferred to a clean Eppendorf tube. The assay was performed on the ELISA plate, according to the manufacturer's protocol. Calculated cAMP levels were normalized to total protein content, quantified using the Pierce 660 nm Protein Assay Kit (Thermo Scientific).

RNA extraction and qRT-PCR

Mice were treated chronically with morphine (10 mg/kg, s.c.) or DPBS for 10 d, and six DRGs (L3–L5 both sides) per mouse were collected 24 h after the last injection into TRI Reagent and homogenized (Sigma-Aldrich, T9424). Total RNA was extracted using chloroform and precipitated by isopropanol. On the next day, after measuring the concentration and purity of RNA with a NanoDrop Spectrophotometer (Thermo Fisher Scientific), total RNA was reversed-transcribed using a High-Capacity RNA-to-cDNA kit (Applied Biosystems). Quantitative real-time PCR (qRT-PCR) was performed using TaqMan Gene Expression Master Mix (Applied Biosystems). Target *hcn2*, *adcy1*, *adcy5*, *adcy8*, and *oprm1* mRNA expression were normalized to a housekeeping gene (*gapdh*). TaqMan probes (Applied Biosystems) used were *hcn2* (Mm00468538_m1), *oprm1* (Mm01188089_m1), *adcy1* (Mm01187829_m1), *adcy5* (Mm00674122_m1), *adcy8* (Mm00507722_m1), and *gapdh* (Mm99999915_g1). For evaluating the mRNA levels of the alternatively spliced variants of six-transmembrane (6TM) *mor*s (m*mor*-1G, m*mor*-1K, m*mor*-1L, m*mor*-1M, and m*mor*-1N), instead of TaqMan qPCR, we applied SYBR green qRT-PCR. The procedure was implemented according to the technical manual of GoTaq qRT-PCR kits (Promega A6010); primers used were as cited in Xu et al. (2014). The mRNA levels of splice variants were normalized to the reference gene, *g3pdh*. qRT-PCR reactions were run in a Roche LightCycler 480 PCR machine. Results were analyzed by the standard $\Delta\Delta_{Ct}$ method.

Patch clamp

DRG neuron culture. After receiving morphine (10 mg/kg) or DPBS for 10 d, WT mice (male C57/BL6, 6–9 weeks old) or conditional HCN2 KO/floxed littermates ($na_V1.8\text{-}cre^{+/-}/fhcn2^{+/+}$ male, 6–10 weeks old) underwent cervical dislocation followed by decapitation 24 h after the last injection, and the spinal cord was opened to expose DRG. DRG

neurons from all spinal levels were collected and incubated in papain (2 mg/ml in Ca^{2+} and Mg^{2+}-free HBSS) and collagenase (2.5 mg/ml in Ca^{2+} and Mg^{2+}-free HBSS) successively for 30 min each at 37°C followed by centrifugation at 1,000 rpm for 5 min and removal of supernatant. In the next step, dissociated DRG neurons were manually triturated in Neurobasal-A medium [Neurobasal-A medium + 0.25% L-glutamine (200 mM) + 2% B-27 + nerve growth factor (NGF, 250 µg/ml)]. Finally, dissociated DRG neurons were centrifuged and plated onto 10 mm coverslips (VWR) that were pre-coated with 0.01% poly-L-lysine and laminin (40 µg/ml) and incubated in Neurobasal-A medium (37°C, 5% CO_2). Whole-cell patch clamp was performed at room temperature (22°C) between 24 and 48 h after DRG neuron isolation.

Solutions and drugs. All patch-clamp experiments were carried out using an extracellular solution comprising (in mM) 140 NaCl, 4 KCl, 1.8 $CaCl_2$, 1 $MgCl_2$, 10 HEPES, 5 glucose (pH adjusted to 7.3 and osmolality 315 mOsm). Intracellular solution contained (in mM) 140 KCl, 1.6 $MgCl_2$, 2.5 MgATP, 0.5 NaGTP, 2 EGTA, and 10 HEPES (pH adjusted to 7.25 and osmolality 290 mOsm) with additions as specified in particular experiments.

Whole-cell patch-clamp recordings. Small DRG neurons (<20 µm diameter) were used for electrophysiological recordings. Whole-cell patch-clamp recordings were performed using an Axopatch 200B patch-clamp amplifier and DigiData 1550 digitizer. All patch pipettes (Science Products) were pulled using a P-97 horizontal micropipette puller (Sutter Instrument) and fire-polished using a MF-900 microforge (Narishige). Final pipette resistance ranged between 2 and 4 MΩ. Pipette offset was corrected before the pipette tip attached to the cell. Before achieving the whole-cell configuration, a gigaohm seal was formed between the pipette tip and the cell surface, and pipette capacitance transients were compensated to zero. After achieving the whole-cell configuration, whole-cell membrane capacitance was measured, followed by series resistance (typically c. 5 MΩ, acceptable maximum 10 MΩ) which was compensated by 40–70%. Cells were held at −60 mV in voltage-clamp mode. The I-Clamp fast mode was applied when switching to current-clamp mode. Whole-cell recordings were sampled at 20 kHz and low-pass Bessel filtered at 2 kHz. Data was acquired and analyzed using Axon pCLAMP 10.4 and Clampfit 10.4 (Molecular Devices). The voltage-clamp mode was used to investigate the voltage dependence of HCN activation. A series of pre-pulse voltage steps from −40 to −140 mV in 20 mV increments for 1.5 s was applied to the cells followed by a fixed 1.5-s-long hyperpolarizing voltage step to −140 mV. Tail currents were recorded to calculate the midpoint activation voltage ($V_{1/2}$). Maximal current density was calculated when the membrane potential was held at −140 mV. The activation curves of HCN channels were fitted using a Boltzmann equation:

$$\frac{It}{It(max)} = \left(1 + \exp^{\left(\frac{V_m - V_{1/2}}{k}\right)}\right)^{-1}$$

where I_t is the current amplitude of the tail current recorded for a given pre-pulse and $I_{t(max)}$ is the maximum current amplitude of the tail current, V_m is the membrane potential of the pre-pulse, $V_{1/2}$ is the midpoint activation voltage at which half the maximal current was evoked, and k is the slope factor. The effect of chronic morphine treatment on voltage dependence of HCN activation was determined by comparing $V_{1/2}$ between control and OIH groups by fitting a linear regression. To further explore the mechanism of how prolonged morphine administration affects HCN activation, drugs were applied as follows: (1) DRG neurons were incubated in extracellular solution containing *D-Phe-Cys-Tyr-D-Trp-Orn-Thr-Pen-Thr* amide (CTOP), a highly selective MOR antagonist, for 10 min (1 µM); (2) guanosine 5′-O-(2-thiodiphosphate) (GDP-β-S, 0.5 mM), an inhibitor of G-protein activation, replaced NaGTP in the intracellular solution; a 5 min gap was allowed after breaking through the cell membrane to allow the compound to enter the cell and bind to and inhibit G-protein activation; (3) DRG neurons were incubated in melittin (100 nM), a G_s inhibitor, for 15 min; and (4) DRG neurons were incubated in pertussis toxin (PTX, 500 ng/ml), a G_i inhibitor, in extracellular solution overnight. The effect of chronic morphine treatment on action potential (AP) firing was explored in current-clamp mode by injecting a family of depolarizing current pulses (0–80 pA in 20 pA increments, 2 s duration (no holding current injected).

Data analysis

All data are presented as mean ± SEM, and group sizes are stated in each figure legend. All figures are plotted with Prism (GraphPad Software Version 8). Statistical significance was determined with SPSS (SPSS Statistics version 26) using Student's *t* test, Mann–Whitney *U* test, chi-square test, one-way ANOVA, two-way ANOVA, three-way ANOVA, and two-way RM ANOVA with Bonferroni's tests (for *post hoc* analysis), as indicated in the corresponding figure legends. Significance is indicated by $^*p < 0.05$, $^{**}p < 0.01$, $^{***}p < 0.001$, and $^{****}p < 0.0001$. A p value of <0.05 was considered significant.

Results

Development of OIH depends on peripheral HCN2 ion channels and MORs

We induced OIH by treating mice with morphine (10 mg/kg daily, s.c.) for 10 d. To track the development of OIH, and also to remove as far as possible any lingering analgesic effect of each previous morphine injection, we measured the mechanical and thermal thresholds 24 h after the previous morphine injection, immediately before the next injection. As Figure 1, *A* and *B*, shows, morphine treatment resulted in a progressive development of mechanical and thermal hyperalgesia that reached a stable level at approximately day 9 (mechanical threshold, from 4.42 ± 0.1 g to 2.46 ± 0.13 g; thermal threshold, from 11.2 ± 0.22 s to 6.39 ± 0.21 s; both $p < 0.001$). Note that in this work we studied the OIH that develops during repeated administration of morphine, while work in some other labs has used the term to describe the hyperalgesia following opioid withdrawal.

To investigate the potential involvement of HCN channels in OIH, we administered the HCN blocker ivabradine to mice that had developed OIH (on day 11 in the above protocol). Ivabradine blocks all four HCN isoforms with almost equal potency (Stieber et al., 2006) but has little interaction with other targets (Young et al., 2014). Moreover, ivabradine is largely CNS excluded (Young et al., 2014; Iacone et al., 2021), and its actions can therefore be attributed to block of peripheral HCN channels. We found that ivabradine (5 mg/kg, s.c.) restored mechanical and thermal withdrawal thresholds 30 min after injection to the same level as measured before morphine administration (mechanical, 4.28 ± 0.14 s at 30 min post-ivabradine vs 4.4 ± 0.16 g, baseline; thermal, 10.59 ± 0.34 s at 30 min post-ivabradine vs 11.07 ± 0.2 s baseline, $p > 0.05$; Fig. 2*A*,*B*), indicating that ivabradine completely reversed both mechanical and thermal OIH. Moreover, the experiment shows that the half-life of ivabradine is ∼2 h, because both mechanical and thermal thresholds were not significantly different from baseline at 30 and 60 min and the effect of ivabradine had reduced to approximately half after 120 min.

We next explored which HCN isoform is responsible for alleviating OIH. We used a targeted *$na_v1.8$*-driven cre-lox strategy (Emery et al., 2011) to delete *hcn2* exons 2 and 3, that code for functionally critical regions of the HCN2 ion channel including the pore loop, in $Na_V1.8^+$ neurons (cKO). $Na_V1.8$ is a member of the voltage-dependent sodium channel family and is specifically expressed in nociceptive primary sensory neurons (Akopian et al., 1996; Stirling et al., 2005). The *hcn2* cKO mice were phenotypically normal and had thermal and mechanical thresholds identical to wild-type mice. Littermates in which loxP sites were intact (*fhcn2*) were used as controls for *hcn2* cKO mice.

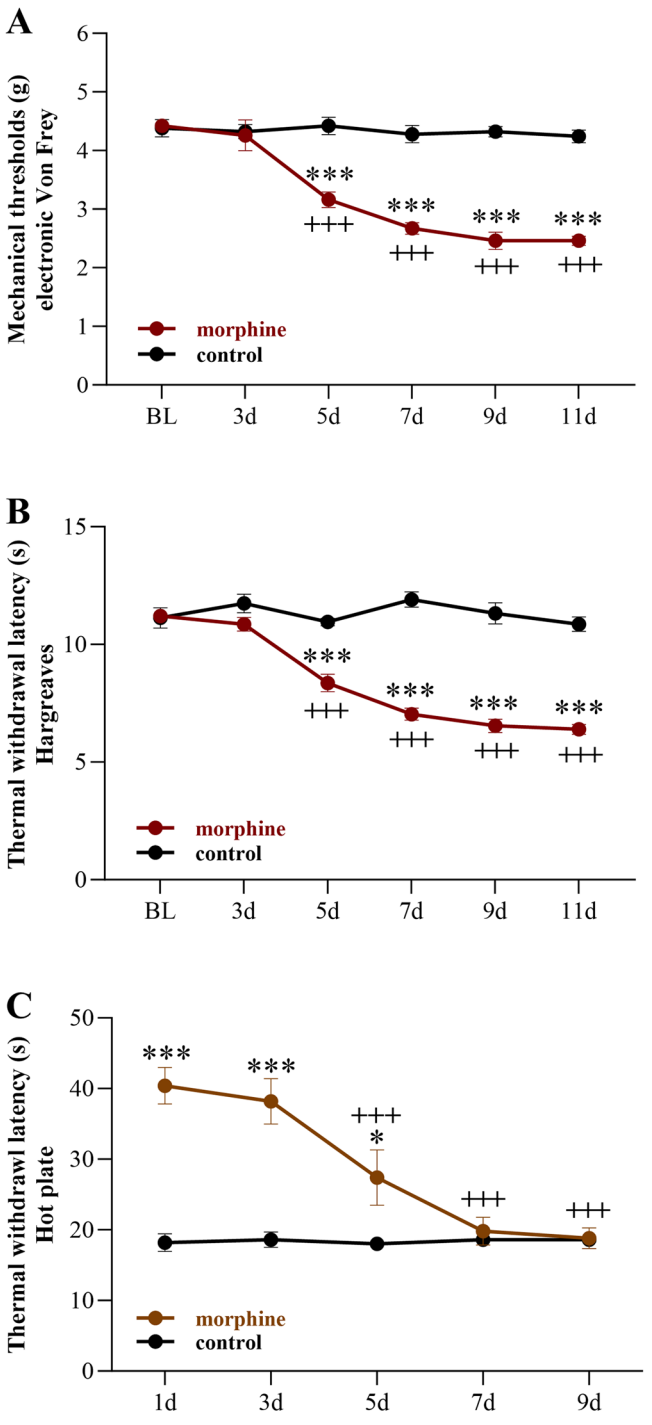

Figure 1. Mouse models of morphine-induced hyperalgesia (OIH, ***A***, ***B***) and tolerance (OIT, ***C***). ***A***, Subcutaneous injection of morphine (10 mg/kg once daily for 10 d) induced a progressive reduction of plantar mechanical threshold, measured 24 h after morphine injection; two-way RM ANOVA followed by Bonferroni's *post hoc* correction ($F_{(2.391,31.084)} = 14.028$; $p < 0.001$) versus BL (+) or control (*). ***B***, Similar decrease of withdrawal latency to thermal stimulation, measured at same time as mechanical threshold; two-way RM ANOVA followed by Bonferroni's *post hoc* correction ($F_{(5,65)} = 27.409$; $p < 0.001$) versus BL (+) or control (*). ***C***, Withdrawal latencies to hotplate thermal stimulation, measured 30 min after morphine injections, declined with repeated morphine administration; two-way RM ANOVA followed by Bonferroni's *post hoc* correction ($F_{(4,32)} = 36.182$; $p < 0.001$) versus BL (+) or control (*). Morphine, $n = 10$; control, $n = 5$. Error bars show mean ± SEM; BL, baseline.

In *hcn2* cKO mice, mechanical and thermal hyperalgesia completely failed to develop during chronic morphine administration. Mechanical thresholds on days 3, 5, 7, 9, and 11 (day 3, 4.58 ± 0.15 g; day 5, 4.6 ± 0.29 g; day 7, 4.3 ± 0.32 g; day 9, 4.3 ± 0.32 g; day 11, 4.25 ± 0.1 g) were not significantly different from baseline (4.4 ± 0.25 g; $p > 0.05$; Fig. 2*C*), and thermal thresholds (10.85 ± 0.6 s, 10.7 ± 0.69 s, 9.87 ± 0.39 s, 10.12 ± 0.51 s, and 10.63 ± 0.12 s, respectively) were likewise unchanged compared with baseline (10.08 ± 0.47 s; $p > 0.05$; Fig. 2*D*). Effectively WT littermate controls (*fhcn2*), however, developed mechanical and thermal hyperalgesia, evident as a significant decline in mechanical thresholds (from 4.44 ± 0.1 to 2.34 ± 0.12 g; $p < 0.001$; Fig. 2*C*) and thermal thresholds (from 10.37 ± 0.31 to 5.48 ± 0.37 s; $p < 0.001$; Fig. 2*D*) in comparison with baseline. These results show that deleting *hcn2* in peripheral nociceptors completely prevents the development of OIH, identifying HCN2 as the crucial HCN isoform that is responsible for initiating and maintaining OIH.

The experiments above support the proposal that OIH is driven exclusively by peripheral HCN2 ion channels. However, we wanted to examine more directly whether there is any role in OIH for centrally located HCN ion channels, by examining the effect on OIH of intrathecal ivabradine injection. In these experiments, shown in Figure 3*C*, we first achieved full development of OIH by morphine injections over 10 d. Ivabradine was then injected intrathecally, with successful injection verified by the presence of the marker methylene blue exclusively within the intrathecal space (see Materials and Methods). Figure 3*C* shows that the intrathecal injection of ivabradine had no effect on OIH, confirming that central HCN channels, at least at the level of the spinal cord, are not implicated in OIH. This result is in striking contrast to the effect of intrathecal injection of ivabradine on OIT (see below).

Finally, we examined the role for peripheral MORs in initiating OIH. When mice were injected with a combination of morphine (10 mg/kg) and a peripherally restricted MOR antagonist (MNB, 5 mg/kg), we found that the development of OIH was completely blocked (day 1 vs day 11, 4.34 ± 0.07 to 4.66 ± 0.17 g for mechanical withdrawal thresholds; 11.75 ± 0.23 to 12.16 ± 0.48 s for thermal withdrawal thresholds; $p > 0.05$; Fig. 2*E*,*F*). Together with the experiments above, these studies show that both peripheral HCN2 ion channels and peripheral MORs are essential for the development of OIH.

OIT is controlled by central HCN channels

The same morphine dosing protocol as is shown in Figure 1*A*,*B* was used to study the development of OIT. The effect of morphine injections on the thermal withdrawal latency in the hotplate test, measured 30 min after morphine injection, shows that the analgesic effect was high after the first morphine injection (Fig. 1*C*; $p < 0.001$ compared with DPBS-injected control group) but slowly declined until it became equal to that of control mice that had not received morphine on day 9 (thermal withdrawal latency 40.4 ± 2.6 s on day1 and 18.8 ± 1.46 s on day 9, $p < 0.001$), showing a clear development of OIT.

We tested whether peripheral HCN channels are implicated in OIT, as they are in OIH, by administering subcutaneous ivabradine. Peripherally administered invabradine is strongly excluded from the CNS (Young et al., 2014). On day 1, injection of ivabradine immediately after morphine had no effect on the analgesia delivered by the morphine injection in the hotplate test, showing that peripheral HCN channels are not involved in acute morphine analgesia (Fig. 3*A*). When OIT had developed fully on day 11, there was likewise no effect of ivabradine in reversing OIT (hotplate withdrawal time 22.00 ± 1.70 s vs 24.80 ± 0.66 s; $p = 0.164$; Fig. 3*A*), showing that peripheral HCN channels are not involved in OIT, in contrast to the abolition of OIH by either ivabradine or a

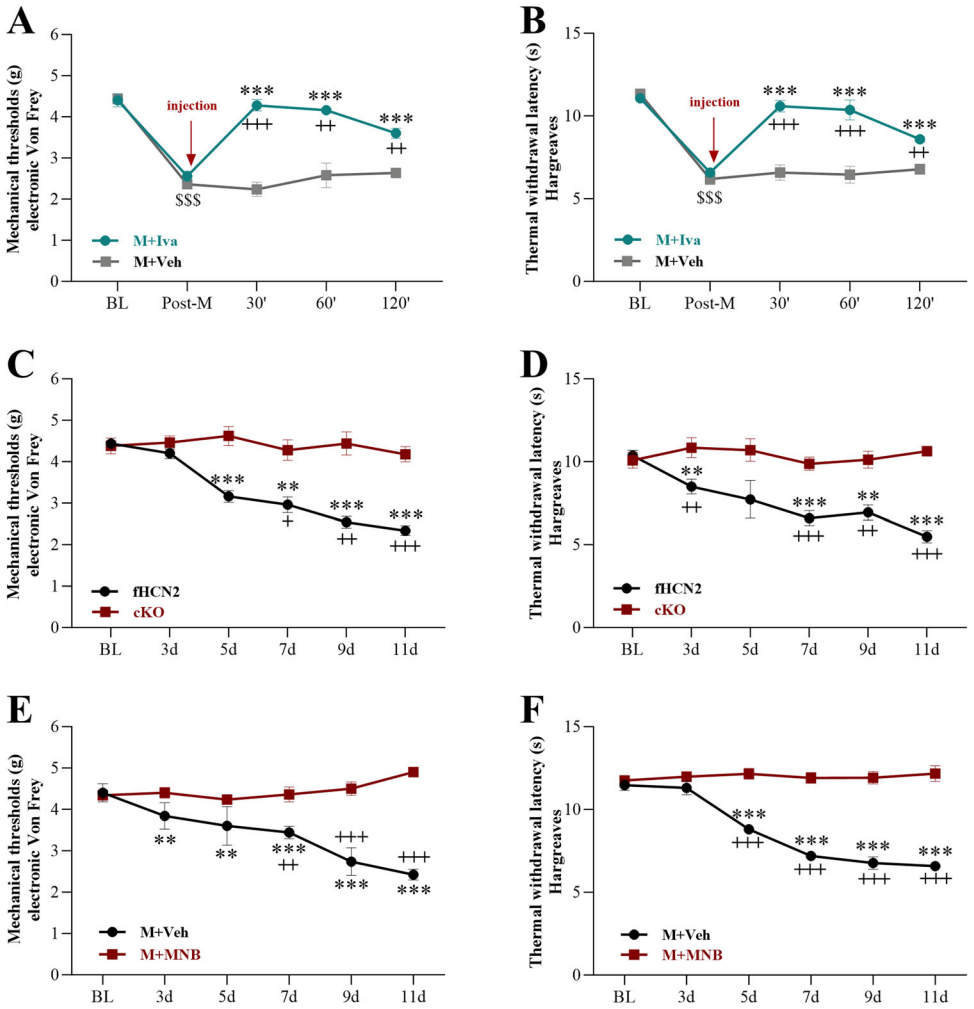

Figure 2. OIH depends on peripheral HCN2 ion channels and MORs. ***A***, ***B***, Peripherally restricted HCN ion channel blocker ivabradine (Iva) reverses OIH. Morphine exposure as in Figure 1 (10 mg/kg, s.c., for 10 d) induced mechanical (***A***) and thermal (***B***) hyperalgesia and injection of ivabradine on day 11 (Iva, 5 mg/kg, s.c.) reversed threshold change when measured 30, 60, and 120 min after injection. Two-way RM ANOVA followed by Bonferroni's *post hoc* correction, mechanical ($F_{(4,32)} = 18.727$; $p < 0.001$), thermal ($F_{(1.838,14.702)} = 15.355$; $p < 0.001$) versus BL ($), day 11 post M + Iva (+) or M + Veh (*); $n = 5$/group. ***C***, ***D***, Genetic deletion of HCN2 in peripheral nociceptive neurons prevents development of OIH. Mechanical and thermal thresholds are unchanged after subcutaneous injection of morphine in mice in which *hcn2* is deleted from $Na_V1.8^+$ neurons (cKO), while a progressive decline of mechanical and thermal thresholds is induced in the control group of f*hcn2*$^{+/+}$ littermates; two-way RM ANOVA followed by Bonferroni, mechanical ($F_{(5,40)} = 11.173$; $p < 0.001$), thermal ($F_{(1.865,14.921)} = 8.121$; $p = 0.005$) versus BL (+) or *hcn2* cKO group (*); $n = 5$ per group. ***E***, ***F***, Peripheral MORs are essential for the development of OIH. Following administration of morphine (10 mg/kg, s.c., once daily) together with the peripherally restricted MOR antagonist MNB (5 mg/kg, s.c., once daily) for 10 d, mechanical and thermal thresholds did not decrease when compared with mice receiving morphine treatment alone; two-way RM ANOVA followed by Bonferroni, mechanical ($F_{(5,40)} = 28.555$; $p < 0.001$), thermal ($F_{(5,40)} = 33.502$; $p < 0.001$) versus BL (+) or M + Veh group (*); $n = 5$/group. Error bars show mean ± SEM; M, morphine; Veh, vehicle; Iva, ivabradine; BL, baseline; fHCN2, *hcn2* floxed controls; cKO, *hcn2* conditional knock-out; MNB, methylnaltrexone bromide.

peripherally targeted HCN2 deletion, as shown above (Fig. 2). There are two distinct possibilities that could explain these results: either OIT develops by a peripheral mechanism that is independent of HCN channels; or a central mechanism, perhaps involving HCN channels, could be involved.

We next investigated whether inhibiting peripheral MORs could affect the development of OIT (Fig. 3*B*). Interestingly, the thermal analgesia delivered by the first morphine injection was reduced by approximately half when peripheral MORs were blocked with MNB, showing that a significant proportion of morphine's analgesic potency is delivered by peripheral MORs (thermal reaction threshold 45 s with morphine alone, but 33.6 ± 4.32 s for morphine + MNB group; $p = 0.03$). However, when OIT had fully developed on day 10 there was no significant difference between the thermal thresholds of mice treated either with morphine alone (21.2 ± 1.46 s) or throughout with morphine plus MNB (20 ± 0.84 s; $p = 0.5$), showing that peripheral MORs are not involved in the development of OIT.

To assess a potential role for central HCN channels in OIT, we delivered an intrathecal injection of ivabradine after OIT had been induced. Figure 3*D* shows the elevated threshold in the hot-plate test 30 min after morphine injection on day 1, and the development of OIT on day 10 of daily morphine injections, followed on day 11 by intrathecal injection of ivabradine immediately before the injection of morphine. OIT was largely reversed by IT ivabradine, when compared with mice that had received intrathecal vehicle (30 ± 1.97 s after IT ivabradine, compared with 14.2 ± 1.02 s with vehicle; $p < 0.001$; Fig. 3*D*). Thus, inhibiting central HCN channels by intrathecal injection of ivabradine largely reversed the development of OIT. This experiment shows that central HCN channels play an important role in OIT, but it does not identify the responsible HCN isoform, because ivabradine inhibits all HCN isoforms approximately equally.

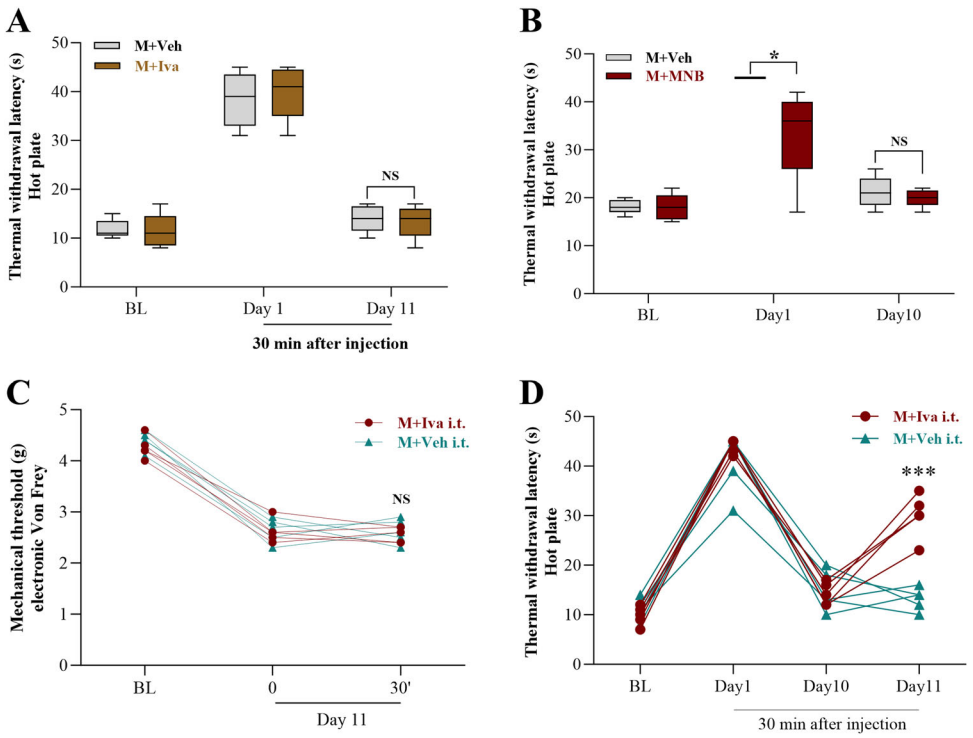

Figure 3. OIT is driven by central HCN channels and MORs. ***A***, Peripheral block of HCN channels by ivabradine does not affect development of OIT. Mice develop morphine tolerance over 10 d morphine treatment, as in Figure 1*C*. Hotplate test shows that peripheral ivabradine injection (5 mg/kg, s.c.) does not affect thermal thresholds either after first morphine injection or after OIT has developed. Two-way RM ANOVA ($F_{(2,16)} = 0.239$; $p = 0.79$) versus M + Veh group, $n = 5$/group. ***B***, Peripheral block of MOR by administration of MNB partially inhibits acute morphine analgesia but does not affect development of OIT. Analgesic effect of morphine was weakened when mice received a combination of morphine and MNB on day 1, two-way RM ANOVA followed by Bonferroni ($F_{(1.243,9.946)} = 5.065$; $p = 0.042$) versus M + Veh group (*); $n = 5$/group. Thermal thresholds are significantly decreased after a 10 d morphine injection, and the decrease is unaffected by co-injection of MNB. Drug dosage: morphine, 10 mg/kg s.c.; MNB, 5 mg/kg s.c.. Error bars represent mean ± SEM. ***C***, Intrathecal injection of ivabradine does not affect OIH. No difference in mechanical thresholds between mice receiving an intrathecal injection of ivabradine (60 µM, 5 µl) and those given the same volume of vehicle, two-way RM ANOVA ($F_{(2,16)} = 0.199$; $p = 0.822$) versus M + Veh i.t. group; both groups $n = 5$. ***D***, Intrathecal injection of ivabradine inhibits OIT. Thermal thresholds increased in OIT mice (day 11) following intrathecal injection of ivabradine (60 µM, 5 µl, red) in comparison with mice with same volume of vehicle injection (green), two-way RM ANOVA followed by Bonferroni ($F_{(1.767,14.135)} = 15.081$; $p < 0.001$) versus M + Veh i.t. group (*), $n = 5$/group. All intrathecal injections verified by methylene blue stain (see Materials and Methods). M, morphine; Veh, vehicle; Iva, ivabradine; MNB, methylnaltrexone bromide; BL, baseline; NS, not significant.

We conclude from these experiments that OIT is driven by central MORs and also by a centrally located member of the HCN family. In this respect, OIT is diametrically opposite to OIH, which as shown above, is driven entirely by MORs and HCN2 ion channels located in peripheral nociceptive neurons.

Peripheral HCN block or deletion of *hcn2* inhibits excitation of second-order neurons

Expression of the immediate early proto-oncogene *c-fos* in second-order neurons of the outer layers of the dorsal horn of the spinal cord is induced by noxious stimulation and provides a sensitive indication of activity in primary nociceptive neurons (Hunt et al., 1987; Harris, 1998; Tsantoulas et al., 2017). After 11 d exposure to morphine, a highly significant upregulation of C-FOS expression was seen in the lumbar dorsal horn (Fig. 4*A*, left). Quantification of C-FOS immunoreactivity indicated that *c-fos* expression increased ~10-fold in OIH mice compared with that in controls, revealing enhanced activation of second-order neurons caused by the induction of OIH (23.44 ± 0.99 vs 2.8 ± 0.43 neurons per section; $p < 0.001$; Fig. 4*A*, right). To assess whether upregulated *c-fos* expression in OIH mice resulted from the activity of HCN2 channels in primary sensory neurons, we examined the C-FOS expression in lumbar sections from mice receiving the HCN ion channel blocker ivabradine (5 mg/kg, s.c.). We found a highly significant reduction of C-FOS 30 min after ivabradine injection (4.96 ± 0.41 neurons per section; $p < 0.001$ in comparison with OIH mice; Fig. 4*A*, right) indicating that block of HCN ion channels inhibited the activity of primary somatosensory neurons and therefore suppressed the induction of C-FOS in second-order spinal neurons with which they synapse. We next examined C-FOS immunoreactivity in the spinal cord of *hcn2* cKO mice to establish whether HCN2 is the critical isoform triggering activity in primary afferent nociceptors. Enhanced C-FOS in second-order neurons was induced by chronic morphine administration in *fhcn2* control mice, but C-FOS is almost entirely lacking in *hcn2* cKO mice following identical morphine treatment (21.4 ± 0.96 vs 2.24 ± 0.35 neurons/sections; $p < 0.001$; Fig. 4*B*). Collectively, these data show that chronic morphine treatment increases the activity of primary nociceptive neurons via HCN2-dependent peripheral nociceptive input.

We showed above that intrathecal injection of ivabradine strongly inhibited OIT. There was, however, no obvious difference in the expression of *c-fos* between mice showing behavioral signs of OIT following chronic morphine injection and mice treated identically that had received an intrathecal ivabradine injection (23.65 ± 1.21 vs 20.45 ± 1.2 neurons per section; $p = 0.068$; Fig. 4*C*). Together with the results above, these experiments show that OIH is driven by HCN2 ion channels that trigger nerve activity in peripheral nociceptive nerve fibers, that in turn triggers *c-fos* expression in second-order neurons of the

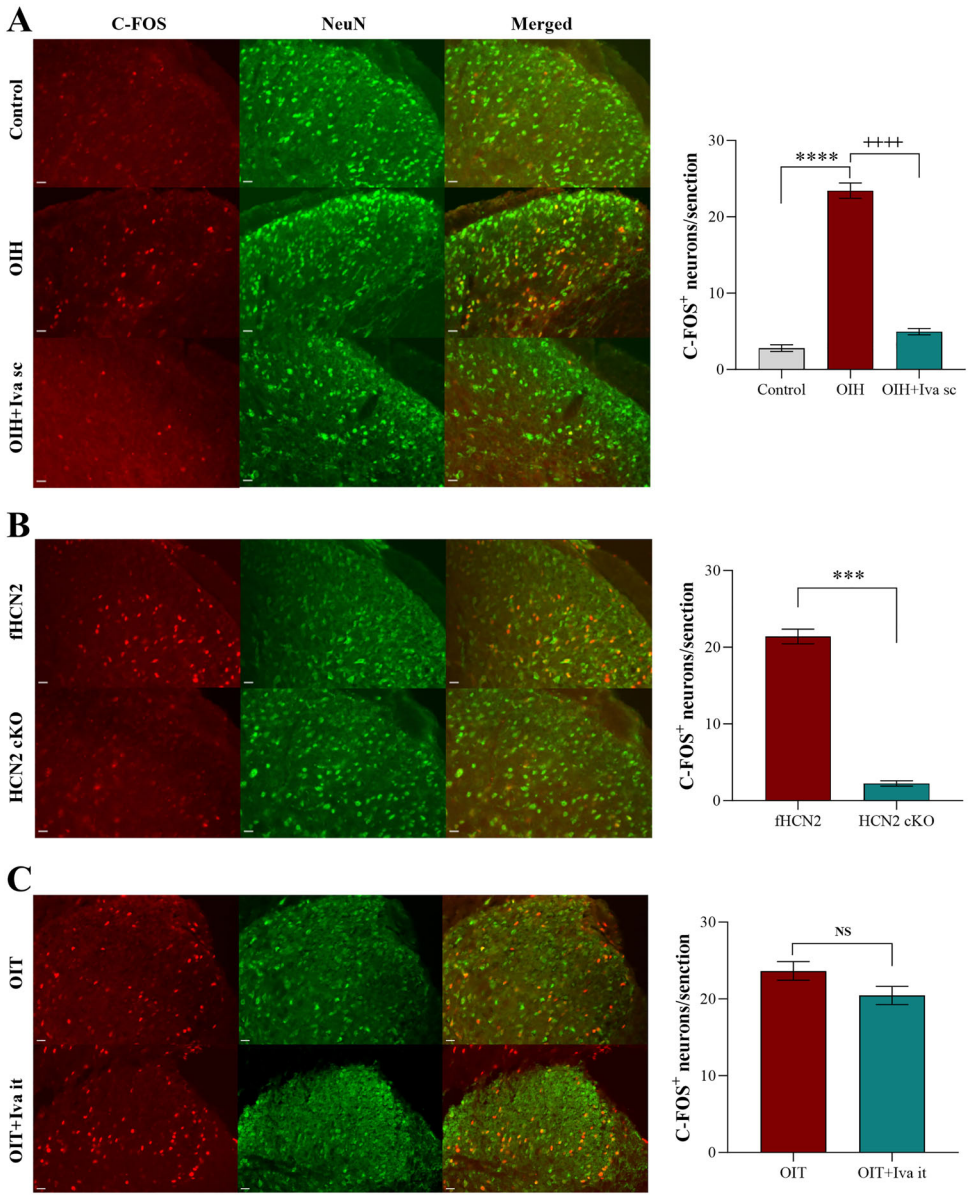

Figure 4. Peripheral HCN block or deletion of *hcn2* inhibits C-FOS expression in second-order neurons of dorsal horn but central HCN block does not. ***A***, Left, Representative images of C-FOS immunofluorescence (left, red) and neuronal marker NeuN (middle, green) in spinal cord dorsal horn in control mice (top row), in mice in which OIH had been induced by 10 d exposure to morphine as in Figure 1 (middle row), or in OIH mice 60 min after injection of ivabradine as in Figure 2*A* (bottom row). ***A***, Right, Quantification of C-FOS-positive neurons in the three groups depicted at the left, one-way ANOVA followed by Bonferroni ($F_{(2,45)} = 201.559$; $p < 0.001$), OIH group vs control group (*) and OIH + Iva sc group (+); $n = 5$ mice, 25 sections/group. ***B***, Left, C-FOS (left, red) and NeuN (middle, green) immunofluorescence in spinal cord dorsal horn in control (*fhcn2*, top) and *hcn2* cKO mice (bottom) following induction of OIH. ***B***, Right, Quantification of C-FOS-positive neurons in the two groups depicted to the left (***$p < 0.001$; Student's unpaired *t* test; $n = 5$ mice; 25 sections/group). ***C***, Left, C-FOS (left, red) and NeuN (middle, green) expression in spinal cord dorsal horn in mice in which OIT had been induced by 10 d exposure to morphine (see Fig. 1*C*), and in OIT mice 30 min after intrathecal injection of ivabradine (see Fig. 3*C*); Right, quantification of C-FOS-positive neurons in the two groups ($p > 0.05$; Student's unpaired *t* test; $n = 5$ mice; 20 sections/group). Error bars show mean ± SEM. All intrathecal injections verified by methylene blue stain (see Materials and Methods). OIH, opioid-induced hyperalgesia; Iva, ivabradine; fHCN2, floxed *hnc2* controls; cKO, *hcn2* conditional knock-out; OIT, opioid-induced tolerance; NS, not significant. Scale bars, 20 µm.

dorsal horn of the spinal cord, while OIT is driven by central HCN ion channels and is unaffected by block or deletion of peripheral HCN2 ion channels. Central delivery of ivabradine therefore blocks OIT but does not significantly affect activity in peripheral nociceptors and does not block OIH.

HCN2 ion channel gating is enhanced in OIH

To directly measure the enhanced excitability of peripheral neurons in OIH, we implemented current clamp on small DRG neurons (diameter < 20 µm), most of which are nociceptive neurons (Treede, 1999; Woolf and Ma, 2007). DRG neurons from mice in which OIH had been induced by chronic morphine exposure were patch clamped after <2 d in culture so as to capture the properties of sensory neurons as close as possible to in vivo.

Current-clamp experiments in Figure 5*A* (left) show enhanced neuronal excitability in response to current injection in DRG neurons following chronic morphine treatment (10 mg/kg, s.c., for 10 d). OIH neurons presented an increased firing frequency of APs following step current injections (0–80 pA) when compared with control neurons ($p < 0.001$; Fig. 5*A*, right), demonstrating enhanced neuronal hyperexcitability following prolonged exposure to morphine.

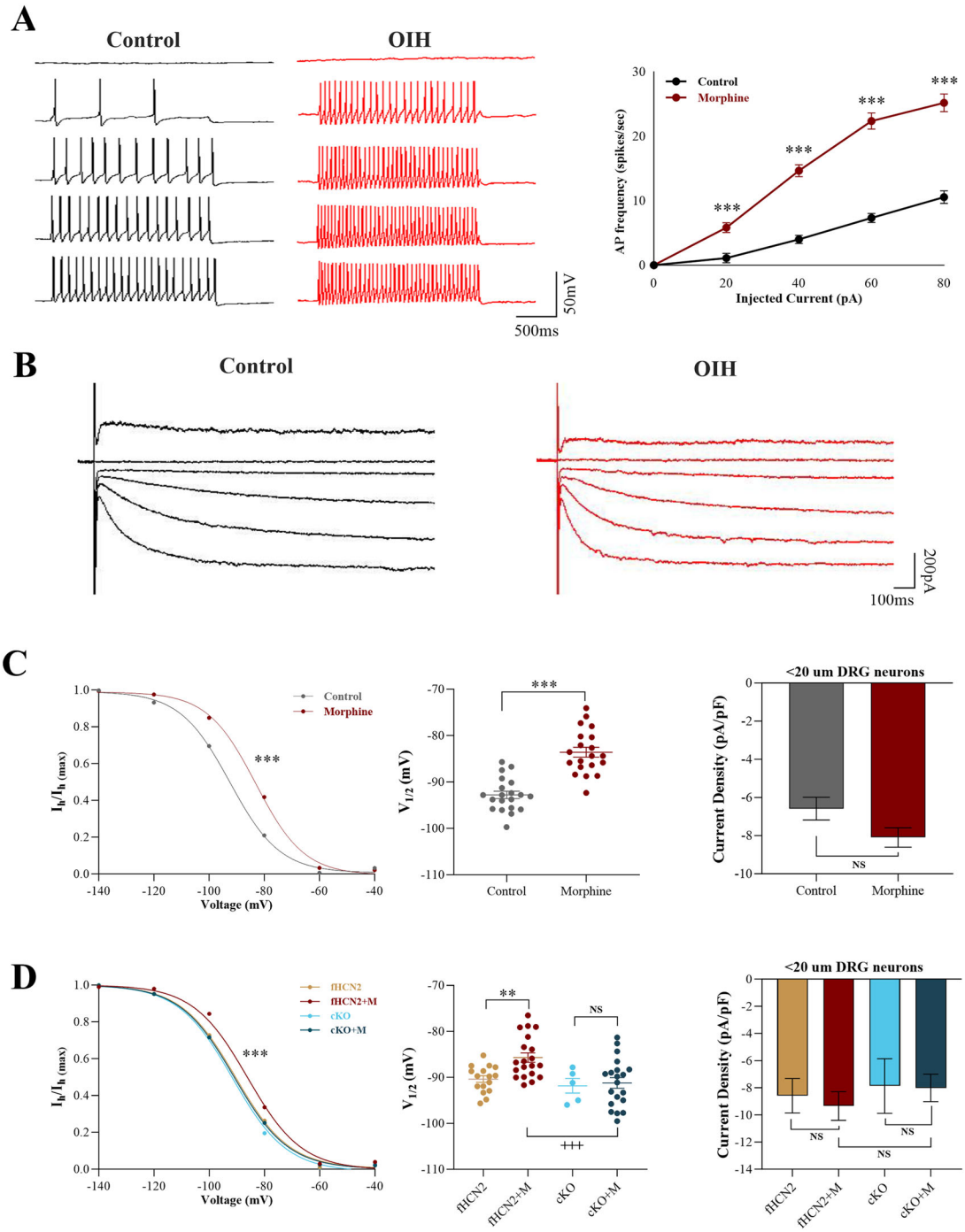

Figure 5. Excitability of small DRG neurons and activation of HCN2 are enhanced by chronic morphine treatment. ***A***, Left, Examples of AP firing evoked by current injection (0–80 pA, duration 2 s) in dissociated small DRG neurons (diameter <20 µm) from control and OIH mice (treated with 10 mg/kg morphine for 10 d; see Fig. 1); Right, analysis of AP firing frequencies showing that firing is increased in neurons from OIH mice, two-way RM ANOVA followed by Bonferroni ($F_{(1.985,35.725)} = 47.466$; $p < 0.001$) versus control group (*); $n = 20$/group; ***B***, Example of voltage-clamp traces of I_h current elicited in response to 20 mV voltage steps, duration 1.6 s from holding potential of −60 mV in neurons from control and OIH mice; ***C***, Left, in neurons from OIH mice, the activation of I_h current underwent a significant depolarizing shift (curves compared with two-way ANOVA; $F_{(1.846,70.129)} = 25.001$; $p < 0.001$). Middle, Shift in half-activation voltage between control and OIH group was $\Delta V_{1/2}$= 9.23 ± 1.33 mV; ***$p < 0.001$; Student's unpaired *t* test. Right, No difference in I_h current density at −140 mV between the two groups (Student's unpaired *t* test; $p = 0.06$), $n = 20$/group; NS, not significant; ***D***, Left, I_h activation was not affected in neurons from *hcn2* cKO mice treated for 10 d with morphine (cKO + M), whereas it exhibited a significant rightward shift in neurons from f/*fhcn2* littermate controls, effectively WT (fHCN2 + M; three-way ANOVA followed by Bonferroni; $F_{(1,204)} = 21.067$; ***$p < 0.001$). Middle, Shift in half-activation voltage ($\Delta V_{1/2}$= −5.51 ± 1.55 mV) following morphine treatment did not occur in neurons from *hcn2* cKO mice treated for 10 d with morphine [two-way ANOVA: fHCN2 vs fHCN2 + M ($F_{(1,57)} = 10.12$; **$p = 0.002$); cKO vs cKO + M ($F_{(1,57)} = 0.084$; $p = 0.773$, NS); fHCN2 + M vs HCN2 cKO + M ($F_{(1,57)} = 15.816$; $^{+++}p < 0.001$)]. Right, Maximum amplitude of I_h current at −140 mV was not affected by morphine treatment or by $Na_V1.8$-targeted deletion of *hcn2* (two-way ANOVA followed by Bonferroni; morphine vs control, $F_{(1,57)} = 0.099$, $p = 0.754$, NS; HCN2 cKO vs WT, $F_{(1,57)} = 0.512$, $p = 0.477$, NS). fHCN2, $n = 16$; fHCN2 + M, $n = 20$; cKO, $n = 5$, cKO + M, $n = 20$. cKO, conditional *hcn2* knock-out; fHCN2, floxed littermate control; M, morphine; NS, not significant.

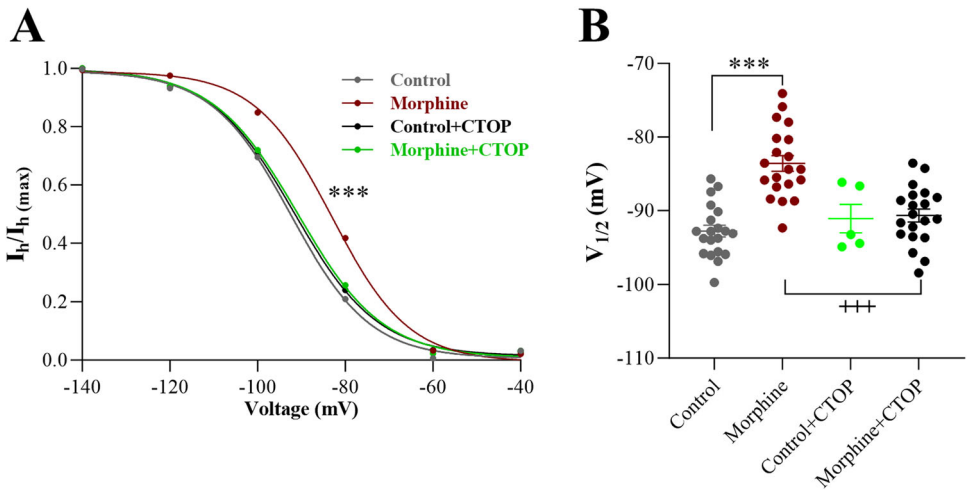

Figure 6. Constitutively active peripheral MORs cause I_h activation in OIH. ***A***, Activation of I_h is MOR dependent. Shift in voltage dependence of I_h activation in small DRG neurons following chronic morphine treatment (10 d; see Fig. 1) was abolished by exposure of neurons for 10 min to the MOR antagonist CTOP; three-way ANOVA followed by Bonferroni ($F_{(1,366)} = 17.416$; $p < 0.001$) versus morphine group (***). ***B***, $V_{1/2}$ value shifted to a depolarized potential following chronic morphine treatment, and the shift was reversed following incubation in CTOP; two-way ANOVA followed by Bonferroni (morphine, $F_{(1,61)} = 15.586$, $p < 0.001$; CTOP, $F_{(1,61)} = 4.846$, $p = 0.032$); control versus morphine, $F_{(1,38)} = 48.018$, $^{*}p < 0.001$; morphine versus morphine + CTOP, $F_{(1,38)} = 26.402$, $^{+}p < 0.001$. Control, morphine, and morphine + CTOP, $n = 20$; control + CTOP, $n = 5$.

The voltage dependence of HCN channel activation was measured by using a series of hyperpolarizing voltage steps (Fig. 5*B*) that activates a slowly developing inward current, I_h, characteristic of HCN channel activation (Young et al., 2014). In small DRG neurons, the time course is consistent with expression of HCN2 or HCN3, that have a similar time course of relaxation, but not with HCN1 which has a much faster time course of activation/deactivation, nor with HCN4 which is much slower (Momin et al., 2008; Emery et al., 2011). HCN2 and HCN3 have been shown to contribute approximately equally to the I_h current in small DRG neurons (Lainez et al., 2019). In Figure 5*C* (left), the location on the voltage axis of the I_h activation curve in DRG neurons from mice treated with chronic morphine injections was significantly shifted in the depolarizing direction when compared with DRG neurons from control animals not exposed to morphine. The $V_{1/2}$ value for control neurons was -92.8 ± 0.8 mV, while after long-term morphine exposure in vivo the $V_{1/2}$ value was -83.57 ± 1.06 mV (shift $\Delta V_{1/2} = -9.23 \pm 1.33$ mV; $p < 0.001$; Fig. 5*C*, middle). Interestingly, the positive shift in I_h was maintained for ~24 h in the absence of morphine following neuronal isolation, implicating a long-term mechanism such as a change in protein expression. Similar maximal densities of HCN current at -140 mV were observed in control and OIH mice (-6.58 ± 0.59 pA/pF vs -8.1 ± 0.51 pA/pF; $p = 0.06$; Fig. 5*C*, right), showing that HCN2/3 expression was not significantly upregulated in OIH.

In DRG neurons from mice in which HCN2 channels have been deleted in $Na_V1.8^+$ neurons (cKO), chronic morphine treatment did not shift the activation curve of I_h ($p < 0.001$; Fig. 5*D*, left), while the $V_{1/2}$ value in *fhcn2* control littermates moved to more positive potentials, as observed with the true WT mice above (fHCN2 + M, -85.7 ± 1.03 mV; cKO + M, -91.21 ± 1.17 mV; $p < 0.001$; Fig. 5*D*, middle). An inward I_h current is still recorded following *hcn2* deletion, but this is due to current carried by HCN3 ion channels that are expressed in all DRG neurons (Lainez et al., 2019). The I_h current density at -140 mV was not different between *fhcn2* mice (effectively WT) and *hcn2* cKO mice receiving 10 d morphine treatment (fHCN2 + M vs HCN2 cKO + M, -9.34 ± 1.06 vs -8.02 ± 1.1 pA/pF; $p = 0.64$; Fig. 5*D*, right). While a reduction of I_h amplitude might be expected when HCN2 is deleted, in other studies a compensatory upregulation of HCN3 expression has been found (Lainez et al., 2019), so that the overall I_h current density is unchanged, consistent with the results shown here.

We next used immunofluorescence staining in mouse DRG sections to confirm whether expression of HCN2 in sensory neurons was changed in OIH (Fig 5-2). In control DRG, HCN2 was expressed in $72.09 \pm 1.16\%$ of all neurons, from colocalization with the nuclear marker DAPI. This finding is consistent with previous studies that had found that HCN2 channels are located in most small-diameter neurons as well as in many larger neurons (Emery et al., 2011). In OIH mice that had received morphine for 10 d, there is no significant difference in the percentage of HCN2-positive neurons ($73.97 \pm 0.97\%$) when compared with the control group ($p = 0.18$; Fig 5-2B, left). There was also no difference between OIH or control neurons in the distribution of HCN2-positive neurons in small, medium, or large neurons ($p = 0.6$; Fig 5-2B, middle). Morphine administration also did not affect HCN2 staining intensity [control, 1.8 ± 0.1 arbitrary units (AU); morphine, 1.84 ± 0.1 AU; $p = 0.15$], and neuronal size had no influence on HCN2 immunoreactivity (slope, $p = 0.67$; intercept, $p = 0.06$; Fig 5-2B, right). Furthermore, qRT-PCR showed that chronic morphine exposure did not alter HCN2 mRNA levels (control vs morphine, 1 ± 0.06 vs 0.98 ± 0.09; expression normalized to housekeeping gene GAPDH; $p = 0.48$; Fig 5-2C). Overall, the above data show that the development of OIH is not due to an upregulation of HCN2 expression or to a shift of expression from (for example) large- to small-diameter neurons.

A noncanonical MOR activates HCN2 ion channels in OIH

To investigate how MORs might communicate with HCN2 ion channels, we first used co-immunohistochemistry, which confirmed that MORs and HCN2 channels are co-expressed in many small DRG neurons (Fig 6-1). As shown in Fig. 5C, a positive shift in the voltage activation curve of I_h was found to be maintained in culture for at least 24 h in the absence of morphine, but the shift was rapidly (<10 min) abolished by incubation with 1 μM CTOP, a potent and selective MOR antagonist (Fig. 6*A*; control, -92.8 ± 0.8 mV; OIH, -83.57 ± 1.06 mV;

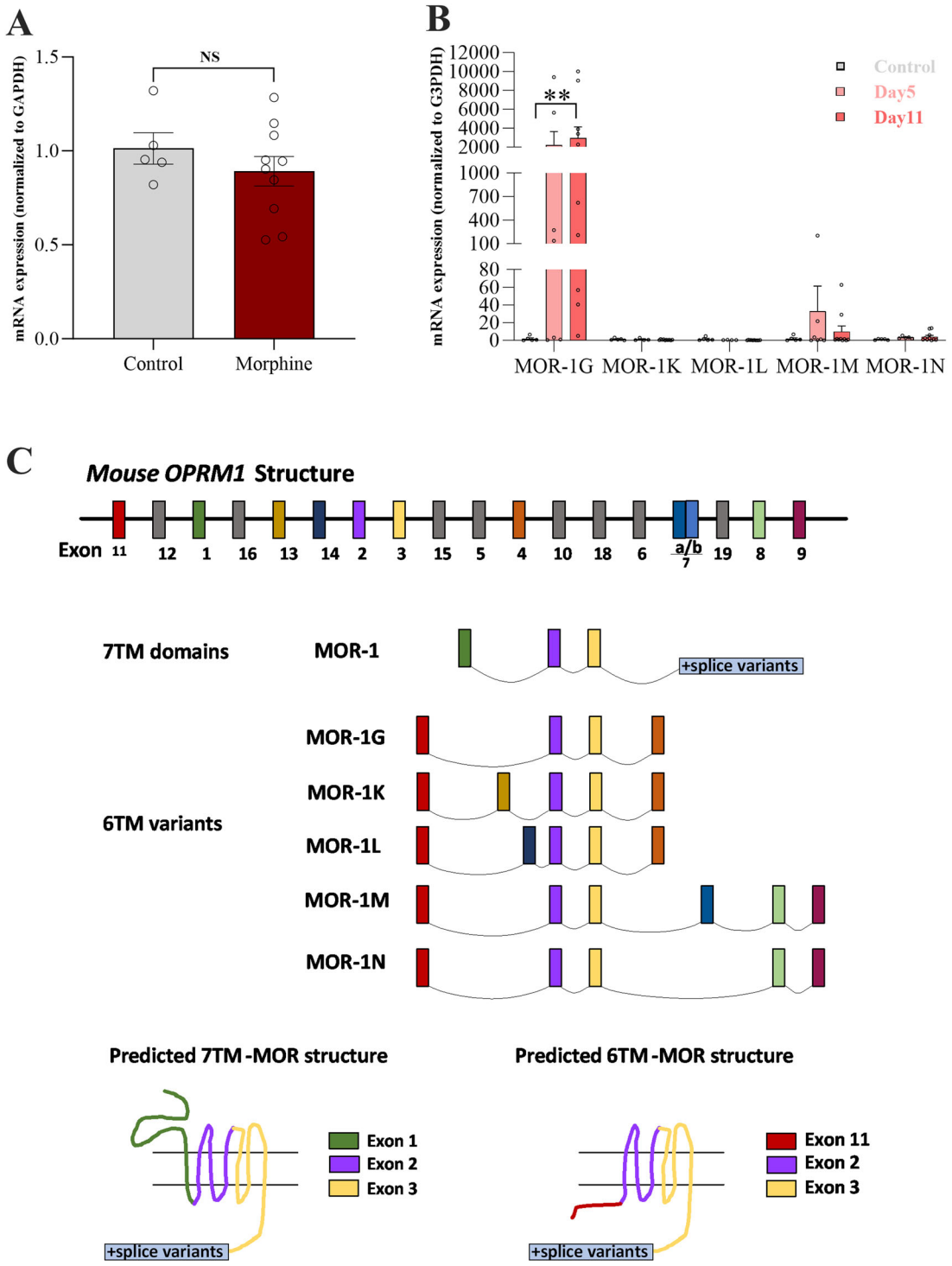

Figure 7. Chronic morphine treatment causes upregulation of expression of mRNA coding for a 6TM MOR. ***A***, Total *mor* mRNA expression does not change significantly in DRG from OIH mice (protocol as in Fig. 1; TaqMan qPCR 24 h after last injection). Control, $n = 5$; morphine, $n = 10$ (Student's unpaired t test; $p > 0.05$). NS, not significant. ***B***, mRNA level of *mor*-1G, a splice variant that codes for a 6TM MOR, increases following chronic morphine treatment. SYBR green qRT-PCR assay for splice variants *mor*-1G, *mor*-1K, *mor*-1L, *mor*-1M, and *mor*-1N. Data shown before morphine injection (left bars) and on day 5 and day 11 following start of daily morphine injection. Significant upregulation observed only for *mor*-1G (**$p < 0.01$; control group vs day 11 group; Mann–Whitney U test); all others non-significant. Control, all $n = 5$; day 5, $n = 7$ for *mor*-1G and 1M, $n = 5$ for *mor*-1N, $n = 4$ for *mor*-1K and 1L; day 11, all $n = 10$. ***C***, Schematic diagram of 7TM and 6TM MOR splice variants. Top, Structure of exons in gene coding for *mor*. Middle, mRNA for canonical 7TM *mor* consists of exons 1–3 followed by several C-terminal splice variants (data not shown). mRNA for 6TM *mor* starts instead with exon 11 followed by several splice variants, *mor*-1G, *mor*-1K, *mor*-1L, *mor*-1M, and *mor*-1N as shown. Bottom, Schematic of transmembrane domain structure of expressed 7TM and 6TM MOR proteins.

CTOP, −90.66 ± 0.88 mV; $p < 0.001$ compared with OIH neurons). These experiments show that (1) a selective MOR antagonist is able to restore the resting activation of HCN2 channels in OIH neurons, confirming that a μ-opioid receptor causes the HCN2 hyperactivity; and (2) the HCN2 hyperactivity persists even in the prolonged absence of morphine. These observations show that expression of a noncanonical MOR, which exhibits constitutive activity in the absence of a μ-agonist, likely

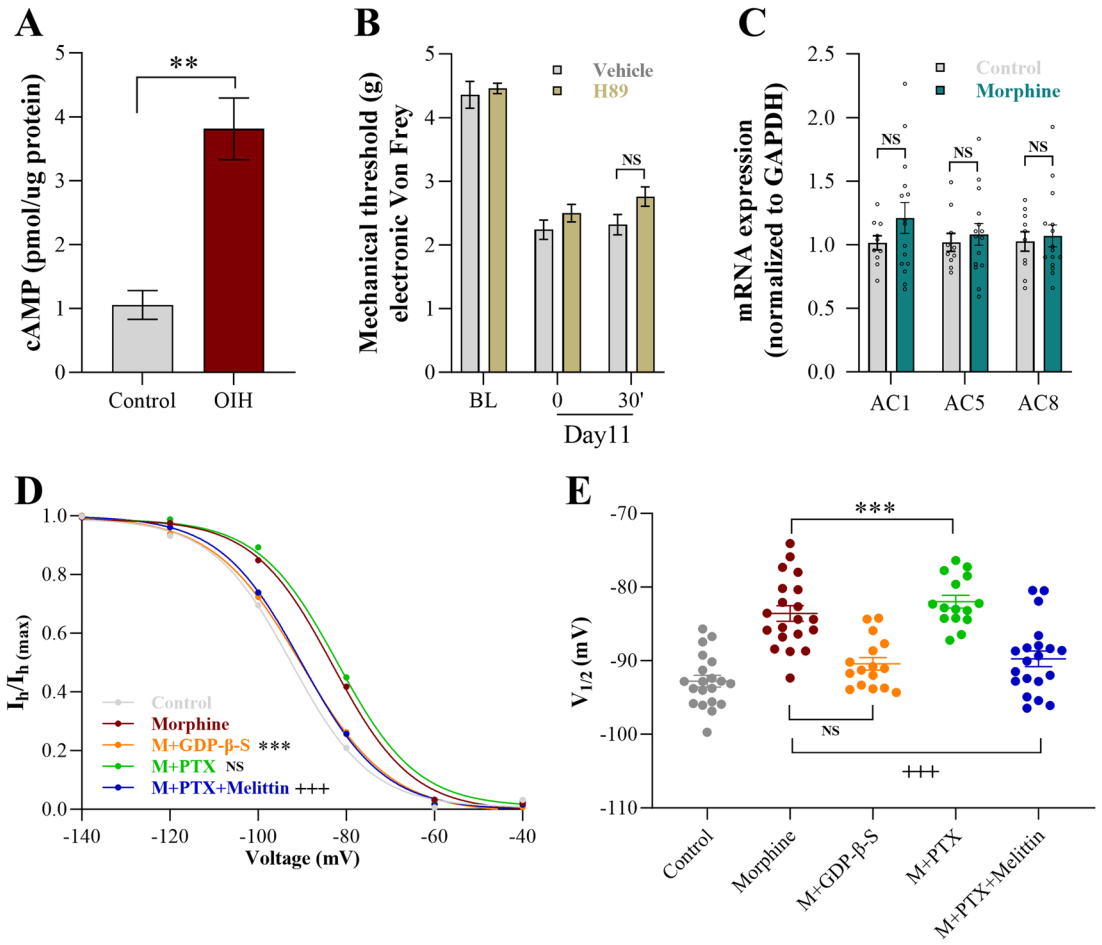

Figure 8. Morphine-induced activation of HCN2 channels depends on the G_s–cAMP signaling pathway. ***A***, Chronic morphine treatment (10 d; see Fig. 1) caused an increase in cAMP in DRG collected 24 h after the last morphine injection (ELISA; $n = 5$/group; $^{**}p < 0.01$; Student's unpaired t test); ***B***, Development of OIH did not depend on PKA. Mechanical hyperalgesia induced by chronic morphine exposure was not reversed by PKA inhibitor H89 (5 mg/kg, s.c., hyperalgesia measured 30 min after injection), two-way RM ANOVA followed by Bonferroni ($F_{(2,16)} = 0.625$; $p = 0.548$); $n = 5$ per group. ***C***, Long-term morphine administration (10 d) did not affect mRNA levels of *adcy1* (AC1), *adcy5* (AC5), or *adcy8* (AC8) measured by qPCR 24 h after the last morphine injection (NS, not significant comparing control and OIH groups; Student's unpaired t test; control, $n = 10$; OIH, $n = 15$). ***D***, Blockade of all G-proteins in OIH neurons by adding GDP-β-S (0.5 mM) to the intracellular patch-clamp pipette solution blocked the positive shift in the activation curve of I_h, two-way ANOVA followed by Bonferroni ($F_{(1,204)} = 46.057$; $p < 0.001$) versus morphine group (*), orange curve. Voltage dependence of I_h activation was not affected when OIH neurons were incubated with G_i-selective inhibitor PTX [500 nM; two-way ANOVA; $F_{(1,198)} = 3.105$; $p = 0.08$ vs morphine group (NS), green curve] whereas the activation curve returned to that observed under control conditions in the presence of PTX (500 nM) plus G_s inhibitor melittin [100 nM; two-way ANOVA followed by Bonferroni; $F_{(1,228)} = 37.204$; $p < 0.001$ vs morphine group (+); blue curve]. ***E***, The shift in I_h half-activation voltage was $\Delta V_{1/2} = 6.86 \pm 1.41$ mV between morphine (OIH) group and morphine + GDP-β-S group and 6.18 ± 1.51 mV between morphine and morphine + PTX + Melittin group, while the $V_{1/2}$ values were not significantly different from morphine group in the PTX-alone group (***, $^{+++}$ both $p < 0.001$; NS, $p = 0.275$; Student's unpaired t test). OIH, opioid-induced hyperalgesia; M, morphine; PTX, pertussis toxin; NS, not significant. Except for the control group, DRG neurons are all from mice following chronic morphine treatment (10 d; see Fig. 1). Control, morphine, and M + Melittin groups, $n = 20$; M + PTX group, $n = 15$; M + GDP-β-S group, $n = 16$.

underlies OIH. Experiments in the next section elucidate the identity of the noncanonical MOR and the signaling pathways that it activates.

Alternative splicing of *mor* mRNA in dorsal root ganglia occurs in OIH

We first measured overall *mor* expression, and we found that the *mor* mRNA levels were not significantly different in sensory neurons from OIH mice compared with control (control vs OIH, 1.01 ± 0.08 vs 0.89 ± 0.08; mRNA expression normalized to GAPDH; $p = 0.36$; Fig. 7*A*). However, this experiment does not exclude a possible change in *mor* exon splicing, and previous work has shown that alternatively spliced 6TM *mor*s can activate a G_s-dependent pathway rather than the normal G_i pathway (Convertino et al., 2015; Oladosu et al., 2015), potentially leading to the activation of HCN2 and thus the development of OIT. We used selective primers to detect mRNA encoding for the five known 6TM *mor*s, as shown schematically in Figure 7*C* (Xu et al., 2014; Liu et al., 2021). Figure 7*B* shows that the mRNA levels of *mor*-1G increased significantly on day 11 in DRGs from the OIH group ($p < 0.001$ compared with control group), showing that the upregulation of expression of a noncanonical 6TM MOR does occur in DRG neurons chronically exposed to morphine.

A sustained elevation of cAMP in dorsal root ganglia mediates OIH

We next explored how the expression of a 6TM MOR could enhance activation of HCN2 channels. A notable feature of HCN channels is that their activation by membrane voltage is directly potentiated by cAMP, due to binding of cAMP to a cyclic nucleotide-binding domain (CNBD) contained in the C-terminal domain of the HCN structure (Zagotta et al., 2003). We therefore assessed the level of cAMP by ELISA, in DRG collected 24 h after

the last morphine injection. As Figure 8*A* shows, following 10 d morphine administration, the concentration of cAMP increased almost fourfold compared with the control group (3.81 ± 0.48 vs 1.05 ± 0.22 pmol/μg protein; $p < 0.001$). We note that cAMP levels in this experiment had remained elevated 24 h after the last morphine injection, when systemic morphine levels would have declined to a low level, in agreement with the sustained elevation of HCN2 activity in the prolonged absence of morphine that was found in electrophysiological experiments in Figures 5 and 6.

Apart from direct binding to HCN ion channels, elevated cAMP could potentially activate PKA and thus modulate ion channels involved in the pain pathway via PKA-mediated protein phosphorylation (Schulz et al., 2008). We therefore tested whether OIH was reduced by an inhibitor of PKA, H89 (5 mg/kg, s.c.) in mice showing fully developed OIH. We found that inhibiting PKA, unlike block of HCN2, did not cause a significant recovery of mechanical thresholds in OIH mice, measured 30 min after H89 injection ($p = 0.082$; Fig. 8*B*), indicating that the elevated cAMP caused by chronic morphine treatment does not induce OIH via a PKA-dependent signaling pathway.

Adenylyl cyclase (AC) super-activation has been reported following chronic morphine treatment (Sharma et al., 1975; Taylor and Fleming, 2001; Bie et al., 2005). AC is present as several isoforms, among which AC1, AC5, and AC8 have been proposed to be involved either in pain responses or in the behavioral effects of morphine (reviewed in Pierre et al., 2009). Quantitative PCR showed that there is no difference in any of the mRNA levels of *ac*1, *ac*5, or *ac*8 in DRG when comparing control and chronically morphine-treated mice (1.01 ± 0.06 vs 1.21 ± 0.12; 1.02 ± 0.07 vs 1.08 ± 0.09; 1.03 ± 0.08 vs 1.07 ± 0.09, respectively; mRNA expression normalized to GAPDH; all $p > 0.05$; Fig. 8*C*). We conclude that the elevated cAMP in DRG neurons following chronic morphine exposure (Fig. 8*A*) does not result from upregulation of expression of AC1, AC5, or AC8.

Activation of HCN2 channels in OIH is G_s dependent

The experiments above do not directly demonstrate that the increased cAMP following chronic morphine treatment results from a switch from activation of G_i, by the canonical 7TM MOR, to activation of a G_s-coupled pathway (Chakrabarti et al., 1998). To establish the G-protein dependence of the shift in voltage dependence of I_h, we replaced GTP (0.5 mM) in the pipette solution with GDP-β-S (0.5 mM), which inhibits the activation of all G-proteins (Suh et al., 2004). As Figure 8*D* shows, loading GDP-β-S into small OIH neurons for 5 min completely inhibited the activation of HCN channels induced by long-term morphine administration, because the $V_{1/2}$ values reverted to the control non-morphine-exposed value (control, −92.8 ± 0.8 mV; OIH, −83.57 ± 1.06 mV; OIH + GDP-β-S, −90.43 ± 0.84 mV; $p < 0.001$ compared with OIH; Fig. 8*E*). This experiment confirms that G-proteins mediate the activation of HCN2 channels following prolonged morphine exposure. To determine whether G_s is critical for OIH, it would have been interesting to apply selective G_s blockers, but to date, no G_s-specific blocker has been developed (Boesgaard et al., 2020). We therefore used melittin, which inhibits G_s and stimulates G_i activity, to assess whether activity of G_s proteins causes the shift in the voltage dependence of HCN2 activation. To remove a possible involvement of G_i, we incubated OIH neurons overnight with pertussis toxin (PTX), that inhibits G_i. We found that PTX alone does not interfere with the activation of HCN2 channels induced by chronic morphine exposure, indicating that G_i proteins are not involved ($V_{1/2}$ values, −83.57 ± 1.06 mV for OIH vs −81.97 ± 0.86 mV for OIH + PTX; $p > 0.5$; Fig. 8*E*). However, we found that PTX + melittin significantly inhibited the positive shift in the activation curve of HCN2 channels in small OIH neurons (−89.75 ± 1.07 mV; $p < 0.001$ compared with OIH neurons; Fig. 8*D*). These results show that the morphine-induced potentiation of function of HCN2 channels in OIH is dependent on the activation of G_s proteins.

Discussion

Location of neurons driving OIH and OIT

Our work supports the proposal that OIH originates from peripheral sensitization, because of the following observations: (1) ivabradine, a peripherally restricted HCN ion channel blocker, completely reverses established OIH (Fig. 2*A*,*B*); (2) selective deletion of HCN2 in $Na_V1.8$-expressing peripheral nociceptive neurons prevents the development of OIH (Fig. 2*C*,*D*); (3) increased AP firing was observed in nociceptive neurons from mice in which OIH had been induced, demonstrating sustained nociceptor hyperexcitability (Fig. 5*A*); (4) C-FOS expression in second-order neurons in outer layers of the spinal dorsal horn, known to be increased by peripheral nociceptive stimuli (Hunt et al., 1987; Harris, 1998), was found to be enhanced in OIH mice, and the enhancement was abolished by either pharmacological block or genetic deletion of HCN2 (Fig. 4); (5) behavioral OIH was prevented by block of primary afferent MORs with the peripherally restricted MOR antagonist MNB (Fig. 2*E*,*F*).

In contrast to OIH, we found that OIT is initiated centrally, because while OIH was completely inhibited by block of either peripheral HCN ion channels or peripheral MORs, the development of OIT was unaffected (Fig. 3*A*,*B*; see also Blomqvist et al., 2022). Intrathecal injection of ivabradine had no effect on OIH (Fig. 3*C*) but inhibited OIT (Fig. 3*D*), confirming a peripheral origin for OIH but a central origin for OIT. Recent work using the less selective HCN blocker ZD7288 has come to a similar conclusion (Yuan et al., 2020). We note, however, that Corder et al. (2017) found that OIT was eliminated by either deletion of MORs in peripheral nociceptors, using a TRPV1-driven Cre-lox strategy, or peripheral block of MORs using MNB, results that are apparently at variance with the above findings and deserve further investigation. Interestingly, we also found that block of peripheral MORs with MNB reduced the acute analgesic efficacy of morphine, showing that peripheral MORs are an important site of action for opioid analgesia (Fig. 3*B*; see also Guan et al., 2008; Jagla et al., 2014; Tiwari et al., 2016; Klein et al., 2018).

The similar time course of onset of both OIH and OIT, together with the block of OIT that was caused by central injection of ivabradine, suggests that morphine-driven activation of HCN2 ion channels may underlie OIT, in a similar way to OIH, but in a central rather than a peripheral location. The location within the CNS of the HCN channels that drive OIT, and the particular HCN isoform involved, were not determined in the present study. The mechanism by which centrally located HCN channels mediate OIT also needs further investigation.

HCN2 ion channels drive OIH

We adopted a two-pronged approach to determining the role of HCN ion channels in OIH and the identity of the particular HCN isoform responsible. Ivabradine is a selective inhibitor of HCN ion channels that is strongly CNS excluded and has few off-target actions (Young et al., 2014) but shows no selectivity among the four HCN isoforms (Stieber et al., 2006). Genetic deletion of

HCN2 by a Cre-lox system that targets deletion to $Na_V1.8$-expressing nociceptors, on the other hand, gives highly selective elimination of HCN2 but has the disadvantage that the gene deletion is present throughout the life of the animal. The two methods in combination enabled unambiguous identification of HCN2 ion channels expressed in $Na_V1.8$-positive nociceptors as being responsible for OIH. These findings challenge the idea that central sensitization initiates or maintains the pain hypersensitivity characteristic of OIH, though central processing may explain the effects on OIH of the CNS interventions that were outlined in the Introduction. Furthermore, we found that central HCN channels do not participate in OIH, owing to the finding that intrathecal injection of ivabradine failed to restore normal withdrawal thresholds in OIH mice (Fig. 3*C*).

Current-clamp experiments showed that nociceptive neurons from OIH mice maintain enhanced excitability for a sustained period of time after isolation (Fig. 5*A*), and voltage-clamp experiments showed that the enhanced excitability was due to a depolarizing shift in the voltage dependence of HCN2 activation (Fig. 5*C*,*D*). The shift in the activation range allows HCN2 ion channels to be more readily activated, thus causing the enhanced neuronal hyperexcitability.

Alternative splicing of MOR determines the switch from opioid analgesia to hyperalgesia

The classic signaling mechanism underlying the alleviation of pain by opioids is via activation of canonical 7TM MORs, causing a G_i-driven reduction of cAMP levels in primary nociceptive neurons and thus a reduction of neuronal excitability. The mechanism is generally attributed to inhibition of voltage-dependent calcium channels and increased activation of K channels (Baillie et al., 2015), though members of the HCN family have also been proposed to be involved (Ingram and Williams, 1994). The overall effect is to inhibit the activity of primary nociceptive afferents and thus to reduce synaptic transmission to second-order neurons in the spinal cord.

Following chronic opioid treatment, however, an opposing *enhancement* of the level of cAMP is observed (Sharma et al., 1975; Chao and Nestler, 2004; Pierre et al., 2009; Chakrabarti et al., 2016). In the present study, we found that chronic morphine treatment increases the cAMP concentration fourfold in primary sensory neurons (Fig. 8*A*) and that this increase is the key driver of enhanced HCN2 activity that underlies OIH (Figs. 5, 6). Elevated cAMP can also trigger PKA-mediated signaling pathways, but we found that the hyperalgesia of OIH was not significantly affected by inhibition of PKA (Fig. 8*B*), indicating at most a limited role for activation of PKA by increased cAMP.

One possible cause of elevated cAMP could be upregulation of AC expression. Several studies have reported that AC1 and AC8 contribute to OIH (Pierre et al., 2009; Chan and Lutfy, 2016; Doucette et al., 2021), and AC5 has also been proposed to be involved in morphine analgesia (Kim et al., 2006). We therefore measured AC1, AC5, and AC8 mRNA expression levels in DRG from OIH mice (Fig. 8*C*), and we found that chronic morphine treatment did not increase expression levels of any of these isoforms. While these studies do not completely rule out upregulation of other AC isoforms as a contributor to OIH, the studies described below support a different mechanism.

Some evidence suggests that AC activity is enhanced following chronic opioid exposure as a result of a switch of opioid receptors from a G_i-coupling mechanism, characteristic of the canonical 7TM MOR receptor, to an unexpected G_s-coupling that has been attributed to expression of alternatively spliced 6TM MORs (Crain and Shen, 2007; Tsai et al., 2009; Chakrabarti et al., 2016; Roeckel et al., 2016). In DRG neurons from mice exhibiting OIH induced by prolonged morphine exposure, we found that cAMP levels were enhanced almost fourfold (Fig. 8*A*), causing an enhanced neuronal excitability (Fig 5*A*) that is mediated by a positive shift in the voltage dependence of HCN2 channels (Fig. 6). Surprisingly, we found that the shift in voltage dependence, once established by chronic morphine exposure, was independent of morphine and was sustained for at least 24 h in culture, but could be reversed by the selective morphine antagonist CTOP (Fig. 6), indicating the expression of an aberrant constitutively active G_s-coupled MOR that, although independent of morphine, nonetheless contains an intact binding site for CTOP. The shift in voltage dependence of HCN2 channels in OIH therefore differs from that seen in other long-term hyperalgesia models, such as those for painful diabetic neuropathy (Tsantoulas et al., 2017) and migraine (Tsantoulas et al., 2022), in which the shift in voltage dependence of HCN2 is maintained in vivo by short-lived inflammatory mediators that elevate intracellular levels of cAMP but are rapidly lost when neurons are isolated.

Several studies have shown that 6TM MORs bind to and activate G_s and are therefore suspected to play a critical role in OIH (Gris et al., 2010; Convertino et al., 2015; Oladosu et al., 2015). In agreement with this view, we found that the mRNA level of *mor*-1G, a splice variant encoding for a 6TM MOR, was significantly elevated after 10 d of morphine injection (Fig. 7*B*), suggesting that protein expression levels of the 6TM MOR coded for by this splice variant would also be upregulated. Moreover, we showed that inhibiting G_s abolishes the enhanced activation of HCN2 channels caused by chronic morphine exposure (Fig. 8*D*,*E*), directly implicating elevated G_s activity in OIH. Our results therefore show that a constitutively activated 6TM MOR variant activates the G_s–AC stimulatory signaling pathway, increasing the intracellular cAMP concentration and consequently potentiating HCN2 function.

In conclusion, we show here that HCN2 in peripheral nociceptors drives peripheral sensitization and the development of OIH through constitutive activation of a 6TM MOR → G_s → cAMP → HCN2 pathway in which expression of an aberrant 6TM MOR is elevated by chronic opioid exposure. An important feature of HCN2 channels is that their block has no effect on withdrawal thresholds in normal animals (Emery et al., 2011; Tsantoulas et al., 2016), but that during OIH or other forms of chronic pain, HCN2 channels switch to a crucial role in pain signaling. Developing a drug which specifically inhibits HCN2 in peripheral nociceptors could therefore be a safe and effective treatment for OIH.

References

Akopian AN, Sivilotti L, Wood JN (1996) A tetrodotoxin-resistant voltage-gated sodium channel expressed by sensory neurons. Nature 379:257–262.

Arout CA, Waters AJ, MacLean RR, Compton P, Sofuoglu M (2019) Minocycline does not affect experimental pain or addiction-related outcomes in opioid maintained patients. Psychopharmacology 236:2857–2866.

Baillie LD, Schmidhammer H, Mulligan SJ (2015) Peripheral μ-opioid receptor mediated inhibition of calcium signaling and action potential-evoked calcium fluorescent transients in primary afferent CGRP nociceptive terminals. Neuropharmacology 93:267–273.

Bie B, Peng Y, Zhang Y, Pan ZZ (2005) cAMP-mediated mechanisms for pain sensitization during opioid withdrawal. J Neurosci 25:3824–3832.

Blomqvist KJ, Dudek KA, Viisanen H, Matlik K, Ahlstrom FHG, Laitila J, Kalso EA, Rauhala PV, Lilius TO (2022) Antagonism of peripheral opioid

receptors by methylnaltrexone does not prevent morphine tolerance in rats. J Neurosci Res 100:329–338.
Boesgaard MW, Harpsoe K, Malmberg M, Underwood CR, Inoue A, Mathiesen JM, Konig GM, Kostenis E, Gloriam DE, Brauner-Osborne H (2020) Delineation of molecular determinants for FR900359 inhibition of G(q/11) unlocks inhibition of Galpha(s). J Biol Chem 295:13850–13861.
Chakrabarti S, Rivera M, Yan SZ, Tang WJ, Gintzler AR (1998) Chronic morphine augments G(beta)(gamma)/Gs(alpha) stimulation of adenylyl cyclase: relevance to opioid tolerance. Mol Pharmacol 54:655–662.
Chakrabarti S, Chang A, Liu NJ, Gintzler AR (2016) Chronic opioid treatment augments caveolin-1 scaffolding: relevance to stimulatory mu-opioid receptor adenylyl cyclase signaling. J Neurochem 139:737–747.
Chan P, Lutfy K (2016) Molecular changes in opioid addiction: the role of adenylyl cyclase and cAMP/PKA system. Prog Mol Biol Transl Sci 137:203–227.
Chan CS, Shigemoto R, Mercer JN, Surmeier DJ (2004) HCN2 and HCN1 channels govern the regularity of autonomous pacemaking and synaptic resetting in globus pallidus neurons. J Neurosci 24:9921–9932.
Chao J, Nestler EJ (2004) Molecular neurobiology of drug addiction. Annu Rev Med 55:113–132.
Convertino M, Samoshkin A, Gauthier J, Gold MS, Maixner W, Dokholyan NV, Diatchenko L (2015) mu-Opioid receptor 6-transmembrane isoform: a potential therapeutic target for new effective opioids. Prog Neuropsychopharmacol Biol Psychiatry 62:61–67.
Corder G, et al. (2017) Loss of mu opioid receptor signaling in nociceptors, but not microglia, abrogates morphine tolerance without disrupting analgesia. Nat Med 23:164–173.
Crain SM, Shen KF (2007) Naloxone rapidly evokes endogenous kappa opioid receptor-mediated hyperalgesia in naive mice pretreated briefly with GM1 ganglioside or in chronic morphine-dependent mice. Brain Res 1167:31–41.
Deng M, Chen SR, Chen H, Pan HL (2019) α2δ-1-Bound N-methyl-D-aspartate receptors mediate morphine-induced hyperalgesia and analgesic tolerance by potentiating glutamatergic input in rodents. Anesthesiology 130:804–819.
Doucette A, Johnson K, Watts V, Klein A (2021) Intrathecal knockdown of adenylyl cyclase 1 attenuates morphine tolerance and withdrawal in mice. J Pain 22:578–579.
Drdla R, Gassner M, Gingl E, Sandkuhler J (2009) Induction of synaptic long-term potentiation after opioid withdrawal. Science 325:207–210.
Emery EC, Young GT, Berrocoso EM, Chen L, McNaughton PA (2011) HCN2 ion channels play a central role in inflammatory and neuropathic pain. Science 333:1462–1466.
Emery EC, Young GT, McNaughton PA (2012) HCN2 ion channels: an emerging role as the pacemakers of pain. Trends Pharmacol Sci 33:456–463.
Ferrini F, et al. (2013) Morphine hyperalgesia gated through microglia-mediated disruption of neuronal Cl^- homeostasis. Nat Neurosci 16:183–192.
Gauss R, Seifert R, Kaupp UB (1998) Molecular identification of a hyperpolarization-activated channel in sea urchin sperm. Nature 393:583–587.
Ghelardini C, Galeotti N, Vivoli E, Norcini M, Zhu W, Stefano GB, Guarna M, Bianchi E (2008) Molecular interaction in the mouse PAG between NMDA and opioid receptors in morphine-induced acute thermal nociception. J Neurochem 105:91–100.
Gong K, Bhargava A, Jasmin L (2016) Glun2b N-methyl-D-aspartate receptor and excitatory amino acid transporter 3 are upregulated in primary sensory neurons after 7 days of morphine administration in rats: implication for opiate-induced hyperalgesia. Pain 157:147–158.
Gris P, et al. (2010) A novel alternatively spliced isoform of the mu-opioid receptor: functional antagonism. Mol Pain 6:33.
Guan Y, Johanek LM, Hartke TV, Shim B, Tao YX, Ringkamp M, Meyer RA, Raja SN (2008) Peripherally acting mu-opioid receptor agonist attenuates neuropathic pain in rats after L5 spinal nerve injury. Pain 138:318–329.
Harris JA (1998) Using c-fos as a neural marker of pain. Brain Res Bull 45:1–8.
Hogan D, Baker AL, Moron JA, Carlton SM (2013) Systemic morphine treatment induces changes in firing patterns and responses of nociceptive afferent fibers in mouse glabrous skin. Pain 154:2297–2309.
Hunt SP, Pini A, Evan G (1987) Induction of c-fos-like protein in spinal cord neurons following sensory stimulation. Nature 328:632–634.
Iacone Y, et al. (2021) Systemic administration of ivabradine, a hyperpolarization-activated cyclic nucleotide-gated channel inhibitor, blocks spontaneous absence seizures. Epilepsia 62:1729–1743.
Ingram SL, Williams JT (1994) Opioid inhibition of Ih via adenylyl cyclase. Neuron 13:179–186.
Jagla C, Martus P, Stein C (2014) Peripheral opioid receptor blockade increases postoperative morphine demands–a randomized, double-blind, placebo-controlled trial. Pain 155:2056–2062.
Kaupp UB, Seifert R (2001) Molecular diversity of pacemaker ion channels. Annu Rev Physiol 63:235–257.
Khomula EV, Araldi D, Levine JD (2019) In vitro nociceptor neuroplasticity associated with in vivo opioid-induced hyperalgesia. J Neurosci 39:7061–7073.
Kim KS, Lee KW, Lee KW, Im JY, Yoo JY, Kim SW, Lee JK, Nestler EJ, Han PL (2006) Adenylyl cyclase type 5 (AC5) is an essential mediator of morphine action. Proc Natl Acad Sci U S A 103:3908–3913.
Klein AH, Mohammad HK, Ali R, Peper B, Wilson SP, Raja SN, Ringkamp M, Sweitzer S (2018) Overexpression of micro-opioid receptors in peripheral afferents, but Not in combination with enkephalin, decreases neuropathic pain behavior and enhances opioid analgesia in mouse. Anesthesiology 128:967–983.
Kouranova EV, Strassle BW, Ring RH, Bowlby MR, Vasilyev DV (2008) Hyperpolarization-activated cyclic nucleotide-gated channel mRNA and protein expression in large versus small diameter dorsal root ganglion neurons: correlation with hyperpolarization-activated current gating. Neuroscience 153:1008–1019.
Lainez S, Tsantoulas C, Biel M, McNaughton PA (2019) HCN3 ion channels: roles in sensory neuronal excitability and pain. J Physiol 597:4661–4675.
Latremoliere A, Woolf CJ (2009) Central sensitization: a generator of pain hypersensitivity by central neural plasticity. J Pain 10:895–926.
Li Y, Wang H, Xie K, Wang C, Yang Z, Yu Y, Wang G (2013) Inhibition of glycogen synthase kinase-3β prevents remifentanil-induced hyperalgesia via regulating the expression and function of spinal N-methyl-D-aspartate receptors in vivo and vitro. PLoS One 8:e77790.
Li T, Wang H, Wang J, Chen Y, Yang C, Zhao M, Wang G, Yang Z (2019) Annexin 1 inhibits remifentanil-induced hyperalgesia and NMDA receptor phosphorylation via regulating spinal CXCL12/CXCR4 in rats. Neurosci Res 144:48–55.
Liu S, Kang WJ, Abrimian A, Xu J, Cartegni L, Majumdar S, Hesketh P, Bekker A, Pan YX (2021) Alternative pre-mRNA splicing of the mu opioid receptor gene, OPRM1: insight into complex mu opioid actions. Biomolecules 11:1525.
Ludwig A, Zong X, Jeglitsch M, Hofmann F, Biel M (1998) A family of hyperpolarization-activated mammalian cation channels. Nature 393:587–591.
Mo J, Lu Z, Peng J, Li XP, Lan L, Wang H, Peng Y (2023) PAG neuronal NMDARs activation mediated morphine-induced hyperalgesia by HMGB1-TLR4 dependent microglial inflammation. J Psychiatr Res 164:150–161.
Momin A, Cadiou H, Mason A, McNaughton PA (2008) Role of the hyperpolarization-activated current Ih in somatosensory neurons. J Physiol 586:5911–5929.
Oladosu FA, Conrad MS, O'Buckley SC, Rashid NU, Slade GD, Nackley AG (2015) Mu opioid splice variant MOR-1 K contributes to the development of opioid-induced hyperalgesia. PLoS One 10:e0135711.
Pierre S, Eschenhagen T, Geisslinger G, Scholich K (2009) Capturing adenylyl cyclases as potential drug targets. Nat Rev Drug Discov 8:321–335.
Reiss D, Maduna T, Maurin H, Audouard E, Gaveriaux-Ruff C (2022) Mu opioid receptor in microglia contributes to morphine analgesic tolerance, hyperalgesia, and withdrawal in mice. J Neurosci Res 100:203–219.
Roeckel LA, Le Coz GM, Gaveriaux-Ruff C, Simonin F (2016) Opioid-induced hyperalgesia: cellular and molecular mechanisms. Neuroscience 338:160–182.
Santonocito C, Noto A, Crimi C, Sanfilippo F (2018) Remifentanil-induced postoperative hyperalgesia: current perspectives on mechanisms and therapeutic strategies. Local Reg Anesth 11:15–23.
Sartiani L, Mannaioni G, Masi A, Novella Romanelli M, Cerbai E (2017) The hyperpolarization-activated cyclic nucleotide-gated channels: from biophysics to pharmacology of a unique family of ion channels. Pharmacol Rev 69:354–395.
Schnorr S, Eberhardt M, Kistner K, Rajab H, Kasser J, Hess A, Reeh P, Ludwig A, Herrmann S (2014) HCN2 channels account for mechanical (but not heat) hyperalgesia during long-standing inflammation. Pain 155:1079–1090.
Schulz DJ, Temporal S, Barry DM, Garcia ML (2008) Mechanisms of voltage-gated ion channel regulation: from gene expression to localization. Cell Mol Life Sci 65:2215–2231.

Sharma SK, Klee WA, Nirenberg M (1975) Dual regulation of adenylate cyclase accounts for narcotic dependence and tolerance. Proc Natl Acad Sci U S A 72:3092–3096.

Stieber J, Wieland K, Stockl G, Ludwig A, Hofmann F (2006) Bradycardic and proarrhythmic properties of sinus node inhibitors. Mol Pharmacol 69: 1328–1337.

Stirling LC, Forlani G, Baker MD, Wood JN, Matthews EA, Dickenson AH, Nassar MA (2005) Nociceptor-specific gene deletion using heterozygous NaV1.8-Cre recombinase mice. Pain 113:27–36.

Suh BC, Horowitz LF, Hirdes W, Mackie K, Hille B (2004) Regulation of KCNQ2/KCNQ3 current by G protein cycling: the kinetics of receptor-mediated signaling by Gq. J Gen Physiol 123:663–683.

Sun J, Chen SR, Chen H, Pan HL (2019) mu-Opioid receptors in primary sensory neurons are essential for opioid analgesic effect on acute and inflammatory pain and opioid-induced hyperalgesia. J Physiol 597: 1661–1675.

Taylor DA, Fleming WW (2001) Unifying perspectives of the mechanisms underlying the development of tolerance and physical dependence to opioids. J Pharmacol Exp Ther 297:11–18.

Tiwari V, et al. (2016) Activation of peripheral mu-opioid receptors by dermorphin [D-Arg2, Lys4] (1-4) amide leads to modality-preferred inhibition of neuropathic pain. Anesthesiology 124:706–720.

Trang T, Al-Hasani R, Salvemini D, Salter MW, Gutstein H, Cahill CM (2015) Pain and poppies: the good, the bad, and the ugly of opioid analgesics. J Neurosci 35:13879–13888.

Treede RD (1999) Transduction and transmission properties of primary nociceptive afferents. Ross Fiziol Zh Im I M Sechenova 85:205–211.

Tsai RY, Tai YH, Tzeng JI, Cherng CH, Yeh CC, Wong CS (2009) Ultra-low dose naloxone restores the antinociceptive effect of morphine in pertussis toxin-treated rats by reversing the coupling of mu-opioid receptors from Gs-protein to coupling to Gi-protein. Neuroscience 164:435–443.

Tsantoulas C, Mooney ER, McNaughton PA (2016) HCN2 ion channels: basic science opens up possibilities for therapeutic intervention in neuropathic pain. Biochem J 473:2717–2736.

Tsantoulas C, Lainez S, Wong S, Mehta I, Vilar B, McNaughton PA (2017) Hyperpolarization-activated cyclic nucleotide-gated 2 (HCN2) ion channels drive pain in mouse models of diabetic neuropathy. Sci Transl Med 9:eaam6072.

Tsantoulas C, Ng A, Pinto L, Andreou AP, McNaughton PA (2022) HCN2 ion channels drive pain in rodent models of migraine. J Neurosci 42: 7513–7529.

Tu H, Deng L, Sun Q, Yao L, Han JS, Wan Y (2004) Hyperpolarization-activated, cyclic nucleotide-gated cation channels: roles in the differential electrophysiological properties of rat primary afferent neurons. J Neurosci Res 76:713–722.

Wang C, Li Y, Wang H, Xie K, Shu R, Zhang L, Hu N, Yu Y, Wang G (2015) Inhibition of DOR prevents remifentanil induced postoperative hyperalgesia through regulating the trafficking and function of spinal NMDA receptors in vivo and in vitro. Brain Res Bull 110:30–39.

Woolf CJ, Ma QF (2007) Nociceptors-noxious stimulus detectors. Neuron 55: 353–364.

Xu J, Lu Z, Xu M, Rossi GC, Kest B, Waxman AR, Pasternak GW, Pan YX (2014) Differential expressions of the alternatively spliced variant mRNAs of the micro opioid receptor gene, OPRM1, in brain regions of four inbred mouse strains. PLoS One 9:e111267.

Young GT, Emery EC, Mooney ER, Tsantoulas C, McNaughton PA (2014) Inflammatory and neuropathic pain are rapidly suppressed by peripheral block of hyperpolarisation-activated cyclic nucleotide-gated ion channels. Pain 155:1708–1719.

Yuan L, Luo L, Ma X, Wang W, Yu K, Shi H, Chen J, Chen D, Xu T (2020) Chronic morphine induces cyclic adenosine monophosphate formation and hyperpolarization-activated cyclic nucleotide-gated channel expression in the spinal cord of mice. Neuropharmacology 176:108222.

Zagotta WN, Olivier NB, Black KD, Young EC, Olson R, Gouaux E (2003) Structural basis for modulation and agonist specificity of HCN pacemaker channels. Nature 425:200–205.

Zeng J, Thomson LM, Aicher SA, Terman GW (2006) Primary afferent NMDA receptors increase dorsal horn excitation and mediate opiate tolerance in neonatal rats. J Neurosci 26:12033–12042.

Zhao YL, Chen SR, Chen H, Pan HL (2012) Chronic opioid potentiates presynaptic but impairs postsynaptic N-methyl-D-aspartic acid receptor activity in spinal cords: implications for opioid hyperalgesia and tolerance. J Biol Chem 287:25073–25085.